NASA Technical Memorandum 4808

A Model for Space Shuttle Orbiter Tire Side Forces Based on NASA Landing Systems Research Aircraft Test Results

John F. Carter, Christopher J. Nagy, and
Joseph S. Barnicki

September 1997

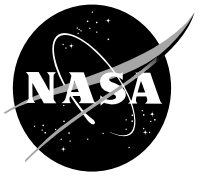

NOTICE

Use of trade names or names of manufacturers in this document does not constitute an official endorsement of such products or manufacturers, either expressed or implied, by the National Aeronautics and Space Administration.

NASA Technical Memorandum 4808

A Model for Space Shuttle Orbiter Tire Side Forces Based on NASA Landing Systems Research Aircraft Test Results

John F. Carter, Christopher J. Nagy, and
Joseph S. Barnicki
Dryden Flight Research Center
Edwards, California

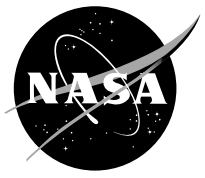

National Aeronautics and
Space Administration
Office of Management
Scientific and Technical
Information Program
1997

CONTENTS

TABLES

FIGURES

ABSTRACT

Forces generated by the Space Shuttle orbiter tire under varying vertical load, slip angle, speed, and surface conditions were measured using the Landing System Research Aircraft (LSRA). Resulting data were used to calculate a mathematical model for predicting tire forces in orbiter simulations. Tire side and drag forces experienced by an orbiter tire are cataloged as a function of vertical load and slip angle. The mathematical model is compared to existing tire force models for the Space Shuttle orbiter. This report describes the LSRA and a typical test sequence. Testing methods, data reduction, and error analysis are presented. The LSRA testing was conducted on concrete and lakebed runways at the Edwards Air Force Flight Test Center and on concrete runways at the Kennedy Space Center (KSC). Wet runway tire force tests were performed on test strips made at the KSC using different surfacing techniques. Data were corrected for ply steer forces and conicity.

INTRODUCTION

Accurately representing landing gear tire forces after touchdown is an essential element for simulation analysis of Space Shuttle orbiter landings. These forces affect the simulated vehicle dynamics during rollout and can play a significant role in landing safety and in tire wear considerations. To measure aircraft tire and wear forces, NASA modified a Convair 990 (CV 990) aircraft (Convair Aircraft, San Diego, California) for use as a tire testing facility called the Landing Systems Research Aircraft (LSRA) (ref. 1). This facility was built to support the Space Shuttle orbiter program by providing tire wear and force data during orbiter landings. The LSRA has a landing gear test fixture between the two main landing gears (fig. 1). This configuration allows the LSRA to expose a test article, such as a tire or landing gear component, to realistic combinations of vertical load, slip angle, and speed during a single test run on various runway surfaces. The LSRA does this by extending the test fixture onto the runway during the rollout phase of a landing.

Simulation models of the Space Shuttle orbiter tire forces exist. These models were developed primarily with the use of data from the NASA Langley Research Center (LaRC), Aircraft Landing Dynamics Facility (ALDF) in Hampton, Virginia (ref. 2). The ALDF gathers data using a hydraulically powered test fixture which moves down a test track with a tire that has one slip angle and one vertical load per test run. The inability of the ALDF to simulate tire heating during a complete orbiter rollout and the absence of any data on the lakebed surface caused uncertainty regarding the tire force models. The LSRA data were used to improve the existing tire force model by

- Measuring tire side and drag forces on dry concrete to verify the LARC model
- Obtaining tire side forces on wet concrete
- Obtaining tire side and drag forces on the Edwards Air Force Base (EAFB), California, lakebed surfaces

The orbiter tire force model based on data from the ALDF (refs. 3 and 4) is under configuration control and is used as the standard model for the Space Shuttle program. The tire force model presented here represents the best available formulation of all the LSRA tire force data. This report recommends implementing the LSRA model as the standard tire force model for the Space Shuttle orbiter program. Hence, documentation is required for background and implementation. This paper provides that documentation.

Preliminary LSRA tire force data were used to create an interim tire force model in June 1994. The interim model was implemented in a limited set of orbiter simulations to generate accurate landing profiles for further LSRA tire wear tests. That model was not widely used or documented. The model described here also is intended to supersede the interim tire force model.

Test methods, data reduction, and formulation techniques for this tire force model are described. A final tabular LSRA orbiter tire side force model for nose gear and main gear tires on concrete and lakebed surfaces is presented. Comparisons to existing tire drag force models are presented; however, no new tire drag force model formulation is given. Wet runway side force is discussed as a percentage of dry runway tire forces.

NOMENCLATURE

ALDF	Aircraft Landing Dynamics Facility, NASA Langley Research Center, Hampton, Virginia

CI	cone index, lb/in^2 from penetrometer tests
DFRC	Dryden Flight Research Center, Edwards, California
EAFB	Edwards Air Force Base, Edwards, California
INS	inertial navigation system
KGS	nautical miles per hour ground speed
KSC	John F. Kennedy Space Center, Florida
LaRC	Langley Research Center, Hampton, Virginia
LSRA	Landing Systems Research Aircraft
WLLGDF	Wright Laboratories Landing Gear Dynamometer Facility, Wright-Patterson Air Force Base, Ohio

TESTBED DESCRIPTION

The test aircraft, a NASA Convair 990 (serial number 10-29, tail number 810) is a high-speed, medium range, low-swept wing jet transport (fig. 1). This aircraft is equipped with four wing-pylon-mounted General Electric (Lynn, Massachusetts) CJ805-23 turbojet engines and a fully retractable tricycle landing gear. The main gear can no longer be retracted with the LSRA modification. This main gear is controlled by dual wheel and columns located in the cockpit. Control surfaces move using a combination of mechanically driven flight tabs and hydraulics. In addition, the basic control system is augmented with a yaw damper which drives the rudder.

The aircraft was modified structurally and mechanically to accommodate the test fixture on the centerline of the aircraft between the main landing gears. The resulting system can simulate vertical load, sideslip, and speed of up to 150,000 lb, 15°, and 240 kn. Vertical load and sideslip control are enhanced using computer feedbacks. The pilot controls the speed using a real-time cockpit error display.

The LSRA can collect either onboard or telemetered data. Loads data are obtained using load cells in the three axes of the test fixture (fig. 2). The drift angle and ground speed of the test tire were calculated from optical velocimeters mounted on the test fixture. Aircraft Euler angles and ground speed were obtained from the inertial navigation system (INS). Accelerations and body axis rates were measured using conventional accelerometer and gyroscopic packages. Stroke position transducers mounted on each landing gear strut provide data for alternate pitch angle and bank angle calculations. Visual data were provided by a real-time video system which had four views of the test tire. For safety considerations, tire temperature and pressure were also instrumented. Data rates for the parameters ranged from 25 to 200 Hz. Reference 1 provides additional details regarding construction and operation of the LSRA.

TEST PROCEDURE

Figure 3 shows a typical landing test sequence. The sequence was initiated after the pilot made a normal CV 990 final approach. After touchdown and derotation, the pilot called for test initiation and used spoilers, thrust reversers, and brakes to maintain the desired speed. For tire force tests, the speed was usually held constant. The test system was activated by an onboard test conductor. The test gear was extended and automatically controlled to match the preprogrammed test profiles of vertical load and slip angle on the test tire. This automatic control made adjustments for flight test uncertainties, such as crosswind (which would change drift angle) and spoiler usage (which would change vertical load of the aircraft). Upon completion of the test, the test gear was automatically retracted. If possible, the aircraft would then rotate and takeoff. Otherwise, the aircraft would come to a full stop on the runway. Test tires were replaced between each test run if extreme wear made it evident that the wear would affect the tire forces during the test. Otherwise, the test tire was not replaced.

Tire force profiles were designed to subject the tires to a number of vertical loads and slip angles at constant speeds. These profiles were not intended to resemble time history test conditions of an orbiter landing. Figure 4 shows a tire force profile plotted with the system response. Vertical loads were held constant long enough for the tire to be steered through three to four discrete angles at a constant velocity. This profile allowed for a variation in slip angle at several vertical loads during each run. The test duration was designed so that the test tire would rotate through at least three times its circumference at each test condition to allow forces to stabilize. Data used to measure tire forces were derived primarily from these parametric test

profiles. In a few cases, additional data points were developed from full-landing tests which were intended for tire wear tests. Quasi-steady state conditions were selected for these additional data points.

TEST CONDITIONS

Tire force tests were performed at two locations: EAFB and KSC. Main gear and nose gear tires were tested according to a matrix of test conditions determined by landing gear engineers at Johnson Space Center (JSC), Houston, Texas, and LaRC. One significant factor in selecting specific conditions was the desire to match test conditions used by ALDF in the original tire force tests, so a direct comparison of forces could be made. The matrix also encompassed the range of test conditions that the orbiter tire would undergo during a nominal landing. Table 1 summarizes the target test conditions for each type of tire and test surface. An examination of the test results shows some small differences between target and actual test conditions.

The EAFB concrete runway (fig. 5(a)) is a relatively smooth surface by the majority of runway standards because wet weather side force is not a primary concern. The surface of this runway has some grooving and pitting, but the sharpness of these surface features is much less severe than that of the KSC runway.

Tire force tests accomplished on the EAFB lakebed were run on lakebed runway 15 (fig. 5(b)), to the right of centerline. This location was far enough to the right of centerline to avoid damaging the orbiter landing area.

Figure 6 represents the surface hardness data from a cone penetrometer taken along the side of runway 15. Hardness measurements were made with a cone penetrometer at 50-ft intervals along the side of the runway. The cone index (CI) is the projected force (lb/in^2) required to drive a square inch area rod 6 in. into the lakebed. Cone index data were used in the computation of an EAFB lakebed drag model. Refer to the Nose Tire Side Forces in Lakebed subsection for additional details.

Figure 7 shows the KSC runway with the surface textures which were present during testing (ref. 5). The center 8000 ft of the runway had the original laterally grooved surface designed to channel off rainwater quickly and to provide side force in wet conditions. The KSC dry concrete main gear tire force data were collected on this surface. At both ends of the runway, 3500 ft were ground down leaving a surface with longitudinal ridges referred to as corduroy. The unground center section and the corduroy section had 10-ft wide test strips which were made using two smoothing techniques: skid abrading and rotopeening. The skid abrading technique involves firing steel shot at the

Table 1. Side and drag tire force test conditions.

Test condition	Surface	Vertical load, lb × 1000	Slip angle, deg	Speed, KGS
Main gear tire forces on dry concrete	KSC concrete	45, 60, 90, 120	0, ±1, ±2, ±4, ±7[a]	50, 160, 190
	EAFB concrete	30, 45, 60, 75, 90, 105, 120	0, ±1, ±2, ±4, ±7[a]	10
Main gear tire forces on EAFB lakebed	EAFB lakebed	45, 60, 90, 120	0, ±1, ±2, ±4, ±6[a]	50, 160, 190
Main gear tire forces on wet concrete	KSC skid abraded on corduroy	45, 60, 90, 120	0, ±1, ±2, ±4, ±7[a]	50, 200
	KSC rotopeened on unground	45, 60, 90, 120	0, ±1, ±2, ±4, ±7[a]	50, 160
Nose gear tire forces on dry concrete	EAFB concrete	10, 30, 50	0, ±1, ±2, ±4	50, 160, 200
Nose gear tire forces on EAFB lakebed	EAFB lakebed	10, 30	0, ±1, ±2, ±4	50, 160, 190

[a]Maximum sideslip angles were not executed at maximum loads.

runway surface. The Rotopeener™ machine uses rotating drums covered with leather flaps which have steel weights, or peens, in them. Both techniques reduce the sharp edges on the surface for a smoother texture. Although never used for tire force testing, a third test strip was formed using a diamond cut saw. The KSC runway was completely resurfaced using a Skidabrader™ machine in October 1994 as a result of the LSRA testing (ref. 5).

Wet runway testing was performed on two KSC surfaces: the corduroy surface with skid abrading treatment and the laterally grooved surface with the rotopeen treatment. Tests on the skid abrader on corduroy sections were accomplished at speeds of 200 and 50 kn. Tests on the rotopeener on laterally grooved surface were conducted at 160 and 50 kn. These combinations were intended to provide the best sampling of an orbiter landing without requiring an excessive number of test points.

Water for the wet runway tests was dispersed from a tanker truck traveling at approximately 25 mi/hr at a rate of 12 gal/sec. NASA LaRC observers estimated the water depth at 0.02 to 0.03 in. All tests were conducted within 5 min of wetting. On the skid abrader on corduroy surface, longitudinal grooves left from the first cutting tended to trap the water on the runway. Conversely, the transverse grooves on the center section drained the water off the surface more quickly. Based on these characteristics, it is unlikely that the water depth was the same for the two surfaces.

Table 2 summarizes the average texture depths on concrete. These texture depths were taken using a grease sample method which measures the area that a given amount of grease will cover a surface (ref. 5).

Table 2. Test surface average texture depth.

Surface	Average texture index[a]
Skid abrader on corduroy (wet runway tests)	0.0096
Rotopeener on unground (wet runway tests)	0.0078
EAFB concrete (nose tire force tests)	0.0067
KSC unground–original (main gear tire force tests)	0.0200

[a]Based on grease sample method.

ANALYSIS TECHNIQUES

Load cell zero biases for the vertical, side, and drag forces were eliminated by subtracting the indicated forces when the test tire was off the ground just before tire extension. This subtraction takes out any external forces, such as aerodynamics on the test fixture, that might bias the results. These forces were then corrected through an Euler angle transformation into the test tire axis (appendix A). Figure 8 provides the test tire axis definition and sign conventions of tire forces and slip angle. Vertical load is perpendicular to the runway; meanwhile, side and drag loads are parallel to the runway, rotated through the steering angle. Inertial navigation system data were used for the pitch angle; meanwhile, the roll angle was calculated from the difference in height of the left and right main gear struts.

Figure 9 shows a time segment of constant vertical load for a typical test run. A table was created by visually averaging the stabilized time history segments of corrected vertical load, slip angle, speed, bank angle, and side force. The dashed lines indicate the chosen discrete values. Data from these observations are presented in appendix B.

Before the appendix B tables could be used for the tire force model, the side force had to be corrected for an effect called conicity. Vertical load exerted through a nonzero bank angle of the wheel results in a flat area of contact between the tire and the runway. This flat area is not perpendicular to the centerline of the tire. With no resistance from the test fixture, this flat area would cause the tire to travel in a circular path similar to the way a cone would roll on a flat surface. The test fixture subjects the tire to side forces which resist the conical path of travel. To calculate this force, an accurate calculation of the total angle from the vertical, or wheel tilt angle, is needed. The equation for the tilt angle is as follows:

$$\text{Wheel tilt} = \text{Aircraft bank angle} + 6.8 \times 10^{-5} \times \text{side load} \quad (1)$$

™Rotopeener is a registered trademark of 3M Company, 3M Center Street, St. Paul, Minnesota 55144-1000.

™Skidabrader is a registered trademark of Humble Eq. Co., 1720 Industrial Drive, Ruston, Louisiana 71270.

The first term is the bank angle of the aircraft as measured by the difference in main gear strut lengths. The second term, 6.8×10^{-5} side load, is the roll deflection resulting from side force of all of the LSRA structure from above the main landing gear struts through and including the orbiter wheel. It was derived during static loads tests conducted at the NASA Dryden Flight Research Center (DFRC), Edwards, California. Once the wheel tilt is calculated, the side force corrected for conicity will be:

$$\text{Corrected side force} = \text{Side force} + 0.01465 \times \text{wheel tilt} \times \text{vertical load} \quad (2)$$

The factor of 0.01465 was derived from specially designed taxi test runs on the LSRA. Both tests were done by vertically loading the tire at 0° slip angle. Periodic steering pulses were placed in each run to prevent mechanical friction from affecting results. A baseline run was performed at 0° bank angle. By inflating the right main gear strut, a bank angle of –1.5° was placed on the aircraft (left wing down), and a second run was made. Similarly, a third run was made with the left strut inflated higher than the right, producing a 1.5° bank angle (right wing down). The side load from the baseline run was subtracted from both of the succeeding runs and divided by the tilt angle. These data were now plotted as a function of the corrected vertical load. A linear fit of that data showed the factor of –0.01465. Appendix B presents data for the roll deflection caused by side force and conicity.

Once the data in appendix B were corrected for conicity, the LSRA Space Shuttle orbiter tire force model was constructed. Side force data were plotted as a function of slip angle for a given vertical load. Solid lines in figure 10 represent the current LSRA tire force model described in this report. Dashed lines represent the ALDF tire force model (refs. 3 and 4), and the circles represent LSRA tire force data collected at that condition. The tire force model described here was created by using a linear fit for all the data between ±3° of slip angle and a tabular curve fit for slip angles beyond ±3°.

An estimation of the ply steer force was made. Ply steer is the side force that a tire produces when it is at a 0° slip angle and is a function of the design of the tire. Although a recognized force bias within the tire manufacturing community, ply steer is usually ignored because of its small magnitude. Yet, these forces become an important factor in computing tire wear when integrated over a complete orbiter rollout. The exact measurement of ply steer forces was hampered by the fact that ply steer values were close to the measurement accuracies of the LSRA system. Consistent biases in the test data, however, indicate that ply steer in orbiter tires is a real phenomenon.

Figure 11 shows ply steer forces which were extracted from several tests conducted at ALDF and Wright Laboratory Landing Gear Dynamics Facility (WLLGDF), Wright Patterson Air Force Base, Ohio. Ply steer values developed from LSRA data are also shown. The solid line represents the current estimate of ply steer based on all the sources of data. It was believed that the ply steer trends of the LSRA at low vertical loads (< 50,000 lb) were not as meaningful as the ALDF or the WLLGDF data because of excessive scatter in the data for those conditions. Ply steer data taken from the ALDF and the WLLGDF showed less scatter and a more consistent trend for the lower vertical loads. At increased vertical loads, the WLLGDF data showed excessive scatter and unreasonable results; meanwhile, the LSRA data showed increased consistency. Therefore, the ply steer model in this report weights the ALDF and WLLGDF data more heavily for the low vertical loads and uses the LSRA trends at high vertical loads. The linear curve fits for main gear tire side forces on dry concrete at the 33,000-, 48,000-, 80,000-, and 94,000-lb vertical loads were altered to reflect the results of this decision. Note that these biases are often well within the uncertainties of the data.

ERROR ANALYSIS

Errors in the tire force data include load cell measurement error and errors from the measurements used in the transformation equations. The latter category includes Euler angles, steering measurements, and drift angle sensors. For example, the equation for vertical load (in part) is as follows:

$$\text{Vertical force}_{\text{runway}} = \text{Vertical force}_{\text{aircraft}} \times \text{cosine(pitch angle)} - \text{drag force}_{\text{aircraft}} \times \text{sine(pitch angle)} + \ldots \text{n.} \quad (3)$$

Appendix A shows the equations for transforming the body axis load cell forces into the test tire axis. An error in the pitch angle measurement creates additional

errors in the runway axis vertical load over and above the errors in the vertical load measurement itself. An accurate representation of the computed vertical force is as follows:

$$\begin{aligned}\text{Vertical force}_{\text{runway}} = {} & (\text{Vertical force}_{\text{true}} \\ & + \text{vertical force}_{\text{error}}) \\ & \times \text{cosine}\,(\text{pitch angle}_{\text{true}} + \text{pitch angle}_{\text{error}}) \\ & - (\text{drag force}_{\text{true}} + \text{drag force}_{\text{error}}) \\ & \times \text{sine}\,(\text{pitch angle}_{\text{true}} + \text{pitch angle}_{\text{error}}) \\ & + \ldots n \end{aligned} \quad (4)$$

By rearranging terms, using small angle approximations, and neglecting products of error terms, an estimate of the contribution of each error may be made.

$$\begin{aligned}\text{Vertical force}_{\text{runway}} = {} & \text{Vertical force}_{\text{true}} \\ & \times \text{cosine}(\text{pitch angle}_{\text{true}}) \\ & - \text{drag force}_{\text{true}} \times \text{sine}(\text{pitch angle}_{\text{true}}) \\ & + \text{vertical force}_{\text{error}} \\ & \times \text{cosine}(\text{pitch angle}_{\text{true}}) \\ & + \text{vertical force}_{\text{true}} \\ & \times \text{cosine}(\text{pitch angle}_{\text{error}}) \\ & - \text{drag force}_{\text{error}} \times \text{sine}(\text{pitch angle}_{\text{true}}) \\ & - \text{drag force}_{\text{true}} \times \text{sine}(\text{pitch angle}_{\text{error}}) \\ & + \ldots n \end{aligned} \quad (5)$$

Table 3 shows the possible errors for the vertical, side, and drag load measurements from each of the measurement components. These errors were developed using the largest component error for each of the items in the transformation equations (shown in column 1). Component error was then propagated through the equations using typical (not maximum) values for the "true" terms shown in equations 3 and 4. Typical values used (based on main gear tire tests) were as follows:

Load, lb		Angle, deg	
Vertical	60,000	Bank	1.0
Side	10,000	Pitch	–1.5
Drag	1,000	Steer	2.0
		Fork	–0.2

The last row in table 3 shows the estimate of error for each of the force values. Note that the affects of slip angle error have been included in the side load error. Because assuming that all errors would occur in the same direction simultaneously is unreasonable, the total error is a root sum square value.

Table 3. Concrete test error contributions.

Error source and magnitude	Resultant vertical load error, lb	Resultant side load error, lb	Resultant drag load error, lb
Vertical load cells, ±3000 lb	±2999	±55	±185
Side load cells, ±500 lb	±9	±500	±0
Drag load cells, ±300 lb	±8	±10	±300
Pitch angle (INS), ± 0.1°	±5	±4	±105
Roll angle (struts), ± 0.2°	±39	±209	±4
Steering angle resolver, ± 0.1°	±0	±352 [a]	±2
Drift angle (optical sensor), ± 0.25°	±0	±867 [a]	±0
Root sum square totals	2999	1083	368

[a]Based on a side force and slip angle value at 63,000 lb vertical load (3467 lb/deg).

The errors presented in table 3 apply directly to testing on concrete runways where optical velocimeters were used to measure drift angle. This optical system is an adaptation of a well-characterized, commercially available system which was accurately calibrated for this application and has an accuracy of 0.25°. For lakebed tests, a mechanical device with a castered aircraft tire was used to measure drift angle. The drift angle accuracy of the mechanical system was estimated at 0.5° although no analysis was completed to verify the accuracy of the mechanical device. If an accuracy of 0.5° is used, the side force error increases to ±1851 lb. However, a 0.5° accuracy has little effect on the vertical or drag loads.

Other errors could be introduced from the 0° tilt angle correction. The 0.01465 factor in the conicity equation was a linear fit of data from LSRA testing. Estimated accuracy of this number is approximately ±0.004. A delta of 0.004 would produce an error in side force of 288 lb with a 1.2° tilt angle and a 60,000-lb vertical load.

RESULTS AND DISCUSSION

These test data were plotted as a function of slip angle for each of the major vertical load and surface combinations used during the test program. These plots have been divided into the following nine categories:

- Main tire side forces on EAFB and KSC dry concrete
- Main tire side forces on EAFB lakebed
- Main tire side forces on KSC wet concrete
- Nose tire side forces on EAFB dry concrete
- Nose tire side forces on EAFB lakebed
- Main tire drag forces on EAFB and KSC dry concrete
- Main tire drag forces on EAFB lakebed
- Nose tire drag forces on EAFB dry concrete
- Nose tire drag forces on EAFB lakebed.

Tire Side Forces

Figures 12 through 35 show side force data for the various combinations of main or nose gear tires and runway surfaces. These plots include the proposed LSRA model, the current ALDF model, and a recently developed lakebed drag model for main and nose gear tires where appropriate. Unless specified otherwise, data presented in these plots have vertical loads ±2000 lb. The following subsections described observations on the data for each category.

Main Tire Side Forces on EAFB and KSC Dry Concrete

Figures 12 through 19 show dry concrete side force data points for various vertical loads plotted as a function of tire slip angle. For the most part, only small differences exist between the ALDF model and the LSRA model. However, the ALDF model does not contain the affects of ply steer. Note that the ALDF curve shown for the 148,000-lb vertical load (fig. 19) has been extrapolated considerably outside the range of the original ALDF test matrix and curve fitting data. The primary benefit of the LSRA model over the ALDF model is the incorporation of the ply steer affects and the improvement of the curve fit at the vertical load and slip angle extremes.

Figure 20 shows the 63,000-lb side force plot from the main tire dry concrete data. These data points encompass speeds ranging from 10 to 200 kn and two surface textures: the EAFB dry concrete and the original unsmoothed dry center section at KSC. Differences between each data set exist, but these differences are relatively small. As a result, all these data sets were used for the LSRA fairings. Although the conclusion that speed and surface affects are small seems surprising, this conclusion had been predicted by ALDF engineers based on previous tire force tests (ref. 6). The fact that the magnitude of the ply steer forces can be smaller than the variance between these data sets is also recognized (appendix B).

Main Tire Side Forces on EAFB Lakebed

Figures 21 through 24 show data from the EAFB lakebed runs for four vertical loads. With two exceptions, the majority of these data matches the model developed for the concrete data surprisingly well. One is the 61,000-lb vertical load plot (fig. 22). The 61,000-lb data appear to be shifted in either side force or slip angle. The shift in these data could be fully explained by the estimated 0.5° accuracy of the mechanical sideslip measuring device (see “Error Analysis” section). The second exception is the low-speed (51 KGS) data from the 124,000-lb vertical load plot (fig. 24). These four side force points show approximately one-half the side force that the LSRA model predicts. Because the majority of these data agree well with the concrete model, the recommendation is to use this model for concrete and lakebed simulations (appendix B).

Main Tire Side Forces on KSC Wet Concrete

Figures 25 through 28 show tire side force measurements for wet concrete on the KSC runway. As discussed in the Test Procedure section, two surfaces were used: the skid abrader on the corduroy section and the rotopeener on the unground center section. Skid abrader tests were performed at 50 and 200 KGS, and

rotopeener tests were performed at 50 and 160 KGS. These test data are relatively limited when compared to the dry concrete tests and were oriented toward testing the conditions most representative of an orbiter landing. Tests accomplished on the skid abraded touchdown zones were conducted at high speeds to simulate orbiter touchdown conditions and low speeds to simulate final rollout. Tests accomplished on the rotopeened center section were intended to match conditions from post derotation to late rollout.

Water depth for the two test surfaces was probably not the same, but both conditions would be representative of the runway condition shortly after a rainstorm. Consistent with pretest expectations, the wet surface tire side force was less for high speeds on the corduroy surface than for the dry surface. Side force for equivalent load and speed test conditions showed greater side force on the rotopeened center section than on the skid abrader or corduroy surface.

Figures 29 and 30 summarize side force measurements showing data as a percentage of dry concrete values. In general, high speeds and low vertical loads tended to decrease the side force the most. To compute wet runway side forces in the simulator, the side force ratios shown in figures 29 and 30 should be applied to the dry concrete forces at the appropriate vertical load, slip angle, and speed conditions (appendix B).

Nose Tire Side Forces on EAFB Dry Concrete

Figures 31 through 33 show nose gear tire data collected at various vertical loads on the EAFB dry concrete runway. These LSRA data values are close to the ALDF model. However, the LSRA data seem to indicate a shallower slope of side forces as a function of slip angle. Note that the ALDF model for the 50,000-lb vertical load is extrapolated well outside the data range originally used to determine the equation. An attempt was made to measure the ply steer affect for the nose gear tire. The magnitude of the side force readings at 0° slip angle was less than the accuracy of LSRA side load cell. Similar to the main gear tire side forces, no speed affects occurred. All data were obtained on the EAFB concrete. As with the main tire dry concrete model, the LSRA nose tire dry concrete model provides improvements at high vertical loads and slip angles.

Nose Gear Tire Side Forces on EAFB Lakebed

These data were generated from force tests using the nose gear tire on the EAFB lakebed (figs. 34 and 35). Note that the majority of these data compare well with the model generated from the concrete tests. Because these tests also used the mechanical side slip device, they are subject to the same 0.5° accuracy limitation as the main gear tire tests on the lakebed. The recommendation is to use the same model for concrete and lakebed simulations.

Tire Drag Forces

Figures 36 through 52 show drag force data for the various combinations of main or nose gear tires and runway surfaces. With the exception of the main gear drag force plot at 145,000-lb vertical load which measured ±4000 lb, all other drag plots had ±2000-lb vertical load.

Drag force data developed by the LSRA for concrete did not warrant changing the existing model. The model used for drag force on a concrete surface was developed by ALDF from earlier track tests with an orbiter tire. The EAFB lakebed model was developed by Gary Kratochvil, International Technology Corporation, and Javier Valencia, Managing Technologies, Incorporated, under contract to JSC. This model was built primarily on early LSRA drag tests using full-stop landing profiles with no slip angle on several lakebed runways. The Kratochvil model is defined by the following equation*:

$$\begin{aligned} \text{Drag} = {} & 4948 - 0.786 \times \text{soil CI} \\ & - 16.995 \times \text{velocity} \\ & + 0.091 \times \text{vertical load} \end{aligned} \qquad (6)$$

The use of full-stop profiles provided data at various combinations of vertical load and speed, but these profiles did not provide the parametric data developed by the later tire force tests. Data provided here can be used to increase understanding of the results from the existing lakebed, but no attempt has been made to update

*Kratochvil, Gary and Javier Valencia, “Ascent/Entry Flight Test Techniques, number 120. Presented as part of an oral briefing given at Johnson Space flight Center, Houston, Texas, December 15, 1994.

that model. Additionally, the model was primarily intended for high-speed (>140 kn) use.

Main Tire Drag Forces on EAFB and KSC Dry Concrete

Figures 36 through 43 also present drag measurements for the main gear tire on several concrete surfaces and at several vertical loads. In general, the LSRA drag measurements were less than those of the ALDF model. However, a significant amount of scatter exists in the LSRA data (fig. 41). While the LSRA values are generally lower than the ALDF values, the magnitude of the differences and the confidence in the LSRA data based on the high degree of scatter does not appear to warrant development of a new model. As was the case with the side forces on concrete, no identifiable speed or surface texture affects occurred.

Main Tire Drag Forces on EAFB Lakebed

Figures 44 through 47 show data gathered from main gear tire tests on the right side of lakebed runway 15. Comparisons between the lakebed drag data and the Kratochvil model show reasonably good correlation at the low vertical loads but less-than-predicted drag at the high vertical loads (figs. 46 and 47). The overprediction results from the fact that the Kratochvil model was originally developed based on LSRA full landing profile runs made on soft soils. That data did not include the hard surfaces found on runway 15. Surface hardness values (CI) for the right side of runway 15 varied from approximately 2500 to 4000 lb/in^2 and indicate a relatively hard surface for soil. (Orbiter engineers were briefed that the model was conservative (predicted increased drag) when the model was delivered.) Note that the speed affects demonstrated by earlier soft-soil tests and predicted by the model are greatly diminished on the hard surfaces.

At high speeds, the Kratochvil model predicts a decrease in drag force with an increase in speed, a nonintuitive result seen in early LSRA full-stop profile test results. Some slip angle affects on drag are apparent although the accuracy of the slip angle is subject to the same limitations as the side force data on the lakebed. No attempt was made to change either the Kratochvil model or develop a new model. However, it is evident that the model could be improved for use on runway 15 by including the latest set of LSRA data.

Nose Tire Drag Forces on EAFB Dry Concrete

Figures 48 through 50 show data from nose gear tire drag force tests conducted on the EAFB concrete runway. While the 0° slip angle magnitude of drag values is comparable to the ALDF model, the variation with tire slip angle does not compare at all. The LSRA data indicate no change in drag with slip angles up to 4°. Unlike data from the main gear tire, data from the nose gear tire tests indicate increasing drag forces as the test speed increases. This increase could not be quantified because the magnitude of these increases is only slightly more than the potential errors in the drag measurement. Note that the ALDF drag curve is extrapolated well outside the original range of vertical loads considered by the ALDF polynomial and should be treated accordingly (fig. 50).

Nose Gear Tire Drag Side Forces on EAFB Lakebed

Figures 51 and 52 show drag data from nose gear tests completed off the right side of EAFB lakebed runway 15. These data indicate a small affect of speed in generating drag where high speeds increase drag values. There appears to be no affect from tire slip angle although the slip angle measurements are subject to the same inaccuracies as side force data. The Kratochvil drag model plots were developed for main gear tires at greatly increased vertical loads and should be used only as a guide. Again, no attempt was made to develop a new lakebed drag model for the nose gear tire.

MATHEMATICAL MODEL

The final LSRA side force model is a table based on vertical load and slip angle. Tables 4 and 5 lists information for main and nose gear tires and apply to concrete and lakebed surfaces. These tables were created from the LSRA curve fits of the data in figures 12 through 35. Note that these data were transformed into the test tire axis and then to zero elastic affects. These tables are based on vertical loads for individual tires and will not work if the dual tire strut vertical load is used. Dual tire strut loads must be reduced to individual tire loads before using these tables because of the nonlinear nature of sideslip data with respect to vertical load.

Table 4. Main gear tire side force model for dry concrete or lakebed, single tire.[a]

	Left steering							Right steering					
	Basic side force												
Slip angle ÷ vertical load	–8	–7	–6	–5	–4	–3	0	3	4	5	6	7	8
0	0	0	0	0	0	0	0	0	0	0	0	0	0
33,000	14,400	14,100	13,600	12,800	11,600	10,372	472	–9,428	–12,300	–14,000	15,300	–16,100	–16,400
48,000	19,500	18,400	17,000	15,200	13,100	11,285	686	–9,914	–14,000	–17,000	–19,500	–21,300	–22,400
63,000	22,700	21,200	19,300	17,000	14,300	11,300	900	–9,500	–12,800	–15,900	–18,600	–20,800	–22,400
80,000	22,500	20,400	18,100	15,700	13,100	10,500	400	–9,800	–12,700	–15,200	–17,600	–19,900	–22,100
94,000	22,300	19,700	17,200	14,600	12,000	9,400	400	–8,600	–11,400	–14,000	–16,600	–19,100	–21,700
111,000	21,400	19,200	16,700	14,000	11,200	8,300	400	–7,600	–10,300	–13,100	–15,700	–18,200	–20,600
126,000	20,600	18,500	16,100	13,500	10,800	8,100	800	–6,400	–9,100	–11,700	–14,300	–16,800	–19,000
148,000	18,900	17,100	14,900	12,400	9,700	7,100	1,000	–5,100	–7,600	–10,100	–12,600	–14,900	–16,900

[a]Wheel tilt angle correction: Side force = basic side force – (0.01465 × tilt angle × vertical load) where tilt angle is positive for clockwise rotation viewed from the rear.

Table 5. Nose gear tire side force model for dry concrete and lakebed, single tire.[a]

	Left Steering				Right steering		
	Basic side force						
Slip angle ÷ vertical load	–8	–4	–2	0	2	4	8
0	0	0	0	0	0	0	0
11,000	5,100	3,500	1,770	–245	–2,260	–4,050	–5,600
31,000	9,100	5,200	2,960	–225	–3,410	–6,500	–10,500
50,000	6,900	2,900	1,920	440	–1,040	–2,550	–6,600

[a]Wheel tilt angle correction side force = basic side force – (0.01465 × tilt angle × vertical load) where tilt angle is positive for clockwise rotation viewed from the rear.

The use of these tables is illustrated next.

Assume the following conditions for a main gear:

Strut vertical load, lb	126,000
Tire vertical load (50/50 share), lb	63,000
Orbiter slip angle, deg	1.3° (nose right)
Orbiter speed, kn	160
Orbiter bank angle, deg	–1.2° (left wing down)

Assuming the 50/50 split for individual tire vertical load, the basic side force on each tire would be –3607 lb. This result is interpolated from table 4 for a 63,000-lb vertical load and a 1.3° slip angle. Note that this amount of side force is experienced by the tire with no tilt angle. In this case, it is assumed that the orbiter bank angle is the entire wheel tilt; that is no strut and axle bending. Based on a bank angle of –1.2° and a vertical load of 63,000 lb, the corrected side force can be calculated:

$$\text{Corrected side force} = \text{Side force} - (0.01465 \times \text{bank angle} \times \text{vertical load}) \quad (7)$$

The corrected side force is then –2499. This correction takes into account the tire side force in the positive direction developed by the vertical force acting through the bank angle. Adding both tires, the resulting side force per strut would be –4998 lb. For a wet runway at KSC, the side force can be multiplied by the factor presented in figures 29 and 30.

SUMMARY AND CONCLUSIONS

Space Shuttle orbiter tire force data were collected using the Landing Systems Research Aircraft (LSRA) and were analyzed in this report. Main gear and nose gear tire forces were analyzed on Edwards Air Force Base (EAFB) and Kennedy Space Center (KSC) concrete surfaces. In addition, main gear tires were used for wet runway testing on KSC skid abraded and rotopeened surfaces. New side force models were produced from the LSRA data.

The models from the LSRA improve the high vertical load and high sideslip angle predictions over the current simulation models which were based on the Aircraft Landing Dynamics Facility (ALDF) test data. The LSRA side force model includes a ply steer correction which was developed from the LSRA, ALDF, and Wright Laboratories Landing Gear Dynamometer Facility (WLLGDF) data.

The LSRA and ALDF dry concrete side force data have little variation with different speeds and runway surfaces. Surprisingly, the data generated by the LSRA on the EAFB dry lakebed also showed only small variations in side force with the data generated from the concrete runways. Such a small amount of variation allows the same model to be used for concrete surfaces at KSC and EAFB as well as for EAFB lakebed site.

Tire drag data were also compared with the existing models for concrete and EAFB lakebed runways. Although some variation occurred in the values of drag from the LSRA and from the existing models, such variations are relatively small, and no new model is proposed.

Limited wet concrete testing was performed on two surfaces on the KSC runway. As measured by side force variations, the wet runway friction ranged from 100 percent of dry runway friction for high vertical loads and low speeds to approximately 30 percent of dry runway friction at low vertical loads and high speeds.

Dryden Flight Research Center
National Aeronautics and Space Administration
Edwards, California, April 14, 1997

APPENDIX A
TIRE FORCE TRANSFORMATION EQUATIONS

These equations were applied to the load cell measurements to transform the measured loads from the load cell axes to the ground-based axes. Measurements include vertical load directly up as well as drag load and side load parallel to the Earth axes and along and perpendicular to the centerline of the tire (fig. 2).

TGNETVERT.M—Corrected test vertical force in pounds. Positive force is up. Corrections are made for transforming the body axis measurements into the test tire axis. The transformation equation is as follows:

$$\begin{aligned} \text{TGNETVERT.M} = {} & \text{VERTFORCE} \times \cos(\text{PITCH}) \\ & \times \cos(\text{BANK}) \\ & - (\text{DRAGFORCE} \times \sin(\text{PITCH}) \\ & \times \cos(\text{BANK})) \\ & + (\text{SIDEFORCE} \times \sin(\text{BANK}) \\ & \times \cos(\text{PITCH}) \end{aligned}$$

TGNETSIDE.M__Corrected test tire side force in pounds. Positive force is left. Corrections are made for transforming the body axis measurements into the test tire axis. The transformation equation is as follows:

$$\begin{aligned} \text{TGNETSIDE.M} = {} & [\text{SIDEFORCE} \\ & - (\text{VERTFORCE} \times \sin(\text{BANK})) \\ & - (\text{DRAGFORCE} \times \sin(\Psi)] / \cos(\Psi) \\ & + \text{VERTFORCE} \times \sin(\text{PITCH}) \\ & \times \sin(\Psi) \end{aligned}$$

TGNETDRAG.M—Corrected test tire drag in pounds. Positive force is aft. Corrections are made for transforming the body axis measurements into the test tire axis. The transformation equation is as follows:

$$\begin{aligned} \text{TGNETDRAG.M} = {} & \text{DRAGFORCE} / \cos(\text{PITCH}) \\ & + (\text{VERTFORCE} \times \sin(\text{PITCH}) \\ & \times \cos(\Psi)) \\ & - \text{VERTFORCE} \times \sin(\Psi) \\ & \times \sin(\text{BANK})) \\ & + (\text{VERTFORCE} \\ & \times \sin(\text{FORKANGLE}) \times \cos(\Psi)) \end{aligned}$$

1. DRAGFORCE = TG_GROS_DRAG – DRAGBIAS
2. $\text{VERTFORCE} = 1.02 \times (\text{TG\_GROS\_VERT} - \text{VERTBIAS})$
3. SIDEFORCE = TG_GROS_SIDE – SIDEBIAS
4. Ψ is the tire steering (not slip) angle.
5. THETA.M was substituted for PITCH when the INS angle measurement failed.
6. BANK = Bank angle of aircraft.
7. DRAGBIAS, VERTBIAS, and SIDEBIAS are biases applied to the load cells as determined from zero force conditions.

PITCH - Aircraft pitch angle in degrees as measured by the inertial navigation system. Nose up is positive.

APPENDIX B
SUMMARY OF FLIGHT DATA AND CONICITY CORRECTIONS

These data were taken by visually averaging the time history data. The load cell data in the time histories were adjusted for zero bias (by subtracting the zero load cell value just before touchdown). The result was transferred to the test tire axis (vertical perpendicular to the runway, side and drag force parallel to the runway, and rotated through the steering angle).

Before these tables could be used for the tire force model, the side force had to be corrected for an affect called conicity. Vertical load exerted through a nonzero bank angle of the wheel results in a flat area of contact between the tire and the runway which is not perpendicular to the centerline of the tire. With no resistance from the test fixture, this flat area would cause the tire to travel in a circular path similar to the way a cone rolls on a flat surface. The test fixture subjects the tire to side forces that resist the conical path of travel. To calculate this force, an accurate calculation of the total angle from the vertical, or tilt angle, is needed.

The equation for the tilt angle is as follows:

$$\text{Wheel tilt} = \text{Aircraft bank angle} + 6.8 \times \text{side load}$$

The first term is the bank angle of the aircraft as measured by the difference in main gear strut lengths. The second term is the side deflection of the test fixture from the bank angle reference to the tire interface with the ground. The second term was derived during static loads tests conducted at the NASA DFRC.

Figure B1 shows a plot from the NASA DFRC static loads test. This graph shows the rotation angles of each of the elements of the test fixture. The dotted line denotes the deflection function used for the elastic portion of the tilt angle.

Once the wheel tilt is calculated, the side force corrected for conicity will be as follows:

$$\text{Corrected side force} = \text{Side force} + 0.01465 \times \text{wheel tilt} \times \text{vertical load}$$

The factor of 0.01465 was derived from specially designed taxi test runs on the LSRA. Both tests were done by vertically loading the tire at 0° slip angle. A baseline run was performed at 0° bank angle. By inflating the right main gear strut, a bank angle of –1.5° was placed on the aircraft (left wing down), and a second run was made. Similarly, a third run was made with the left strut inflated higher than the right, producing a 1.5° bank angle (right wing down). The side load from the baseline run was subtracted from the two succeeding runs and divided by the tilt angle.

Figure B2 shows these data plotted as a function of the corrected vertical load. Periodic steering pulses were placed in each run to prevent mechanical friction from affecting results. These pulses are the reason for the apparent scatter in the data. A linear fit of that data showed the factor of –0.01465. Similar tests were done at the ALDF, and two data points are also shown on this plot. Side loads corrected for conicity are presented in the far right column of tables B1–B5.

Table B1. Data from main tire dry concrete tire force tests.

Vertical load, lb	Slip angle, deg	Speed, KGS	Bank angle, deg	Side force, lb	Drag force, lb	Corrected side load for conicity, lb
			EAFB			
33,000	–0.65	10	0.0	2,100	400	2,169.04
33,000	1.35	10	0.0	–4,800	400	–4,957.80
33,000	–2.55	10	0.1	8,200	400	8,517.92
33,000	–0.65	10	0.1	2,100	400	2,217.38
63,000	–0.65	10	0.1	4,300	700	4,662.17
63,000	1.35	10	0.1	–4,200	800	–4,371.30
63,000	–2.55	10	0.4	9,400	800	10,359.13
63,000	–0.65	10	–0.2	3,700	700	3,747.62
94,000	–0.55	10	0.3	1,700	1,300	2,272.32
94,000	1.35	10	0.3	–3,300	1,200	–3,195.89
94,000	–2.65	10	0.8	6,700	1,400	8,429.09
94,000	–0.55	10	–0.1	3,500	1,300	3,690.04
125,000	–0.65	10	0.2	2,100	1,700	2,727.75
125,000	1.25	10	0.1	–1,800	1,800	–1,841.02
125,000	–2.55	10	0.2	5,800	2,200	6,888.50
125,000	–0.75	10	0.0	2,000	1,800	2,249.05
63,000	–0.65	10	0.2	2,900	700	3,266.60
63,000	1.35	10	0.1	–3,800	700	–3,946.20
63,000	–2.55	10	0.5	8,500	800	9,494.94
63,000	–0.65	10	0.2	3,000	700	3,372.87
33,000	0.05	10	–0.2	600	200	523.03
33,000	1.05	10	–0.3	–3,200	200	–3,450.23
33,000	2.95	10	–0.3	–10,200	300	–10,680.36
33,000	5.95	10	–0.4	–15,000	300	–15,686.50
33,000	–0.95	10	–0.3	4,400	300	4,399.61
33,000	–2.15	10	–0.3	6,800	300	6,878.51
33,000	–3.15	10	–0.3	10,000	300	10,183.71
33,000	–5.05	10	–0.3	13,000	300	13,282.33
33,000	–8.0	10	–0.3	15,100	300	15,451.37
49,000	0.05	10	–0.3	1,100	400	938.34
49,000	0.95	10	–0.3	–2,700	400	–3,047.15
49,000	3.05	10	–0.4	–10,800	500	–11,614.33

Table B1. Continued.

Vertical load, lb	Slip angle, deg	Speed, KGS	Bank angle, deg	Side force, lb	Drag force, lb	Corrected side load for conicity, lb
			EAFB			
49,000	5.95	10	–0.4	–18,500	700	–19,690.20
49,000	–1.05	10	–0.4	5,400	500	5,376.45
49,000	–1.95	10	–0.4	8,300	500	8,418.01
49,000	–2.95	10	–0.4	11,300	500	11,564.46
49,000	–5.05	10	–0.4	16,000	600	16,493.88
49,000	–7.95	10	–0.4	19,500	700	20,164.73
64,000	0.05	10	–0.4	1,800	800	1,539.72
64,000	0.95	10	–0.4	–1,600	800	–2,077.05
64,000	2.95	10	–0.5	–10,800	900	–11,957.37
64,000	5.95	10	–0.5	–19,500	1,300	–21,212.06
64,000	–0.95	10	–0.4	4,800	600	4,730.99
64,000	–2.05	10	–0.5	8,000	600	8,041.25
64,000	–3.05	10	–0.5	11,200	700	11,445.28
64,000	–4.95	10	–0.5	17,000	900	17,615.07
64,000	–7.75	10	–0.4	21,500	1,500	22,495.73
80,000	0.05	10	–0.6	1,100	900	484.47
80,000	0.85	10	–0.7	–2,500	900	–3,519.64
80,000	2.95	10	–0.8	–9,000	1,200	–10,654.86
80,000	–0.95	10	–0.7	4,600	900	4,146.20
80,000	–2.05	10	–0.7	7,600	1,000	7,385.29
80,000	–2.95	10	–0.7	10,200	1,100	10,192.50
80,000	–4.85	10	–0.7	15,000	1,300	15,375.04
96,000	–0.05	10	–0.7	1,300	1,300	439.85
96,000	1.05	10	–0.8	–700	1,300	–1,892.06
96,000	2.95	10	–0.9	–7,500	700	–9,483.02
96,000	–0.95	10	–0.8	4,600	1,400	3,914.80
96,000	–1.95	10	–0.8	7,000	1,400	6,544.33
96,000	–2.95	10	–0.8	10,000	1,500	9,831.23
96,000	–4.95	10	–0.7	14,600	2,100	15,011.79
111,000	–0.05	10	–1.0	2,400	2,300	1,039.24

Table B1. Continued.

Vertical load, lb	Slip angle, deg	Speed, KGS	Bank angle, deg	Side force, lb	Drag force, lb	Corrected side load for conicity, lb
			EAFB			
111,000	0.95	10	–1.0	–100	2,600	–1,737.21
111,000	2.85	10	–1.1	–5,900	2,900	–8,341.18
111,000	–0.95	10	–0.9	4,300	2,400	3,311.95
111,000	–2.05	10	–0.8	6,500	2,400	5,917.84
127,000	0.05	10	–0.7	1,900	1,900	838.00
127,000	1.05	10	–0.4	–300	1,900	–1,082.18
127,000	3.05	10	–0.2	–5,600	2,300	–6,680.61
127,000	–0.95	10	0.0	3,300	2,000	3,717.51
127,000	–1.95	10	0.0	4,900	1,800	5,519.94
127,000	–2.95	10	0.0	7,500	2,300	8,448.88
127,000	–4.75	10	0.0	11,800	2,900	13,292.91
147,000	–0.05	10	0.0	900	2,800	1,031.80
147,000	1.05	10	0.0	–300	3,200	–343.93
147,000	3.15	10	0.0	–4,600	3,700	–5,273.63
33,000	0.05	10	–0.3	600	100	474.69
33,000	1.05	10	–0.3	–3,400	200	–3,656.81
33,000	2.95	10	–0.3	–9,000	200	–9,440.91
33,000	6.05	10	–0.3	–14,600	300	–15,225.00
33,000	–0.85	10	–0.3	3,500	200	3,470.03
33,000	–1.85	10	–0.3	6,600	300	6,671.94
33,000	–2.85	10	–0.3	9,400	100	9,563.99
33,000	–4.85	10	–0.3	12,300	100	12,559.32
33,000	–7.85	10	–0.3	14,600	100	14,934.93
49,000	0.15	10	–0.3	500	300	309.05
49,000	1.05	10	–0.4	–2,800	300	–3,223.82
49,000	3.15	10	–0.4	–10,200	500	–10,985.04
49,000	6.05	10	–0.4	–17,800	700	–18,956.03
49,000	–0.95	10	–0.4	4,500	300	4,432.52
49,000	–1.85	10	–0.4	7,500	300	7,578.96
49,000	–2.85	10	–0.4	10,500	40	10,725.40

Table B1. Continued.

Vertical load, lb	Slip angle, deg	Speed, KGS	Bank angle, deg	Side force, lb	Drag force, lb	Corrected side load for conicity, lb
			EAFB			
49,000	–4.95	10	–0.4	15,500	500	15,969.47
49,000	–7.85	10	–0.4	19,000	600	19,640.32
64,000	0.05	10	–0.4	700	900	369.59
64,000	1.05	10	–0.4	–1,900	900	–2,396.18
64,000	3.15	10	–0.5	–9,500	1,000	–10,574.49
64,000	6.05	10	–0.6	–18,500	1,300	–20,242.06
64,000	–0.85	10	–0.4	4,500	700	4,411.87
64,000	–1.85	10	–0.4	8,000	700	8,135.01
64,000	–2.85	10	–0.4	10,500	800	10,794.41
64,000	–4.85	10	–0.4	15,700	1,000	16,325.94
64,000	–7.85	10	–0.3	21,200	1,300	22,270.36
80,000	0.05	10	–0.5	900	1,000	385.73
80,000	1.05	10	–0.6	–2,200	900	–3,078.53
80,000	3.15	10	–0.7	–8,600	1,300	–10,105.79
80,000	–0.85	10	–0.6	4,100	1,000	3,723.55
80,000	–1.85	10	–0.6	6,600	1,000	6,422.79
80,000	–2.85	10	–0.6	9,700	1,100	9,769.85
80,000	–4.65	10	–0.5	14,600	1,400	15,177.56
95,000	0.05	10	–0.6	1,100	1,300	369.05
95,000	1.15	10	–0.6	–2,000	1,400	–3,024.33
95,000	3.25	10	–0.8	–7,200	1,700	–8,994.80
95,000	–0.95	10	–0.7	4,000	1,300	3,404.33
95,000	–1.85	10	–0.8	6,600	1,700	6,111.22
95,000	–2.85	10	–0.8	9,500	1,900	9,285.67
95,000	–4.85	10	–0.6	14,100	2,400	14,599.36
111,000	0.05	10	–1.1	2,100	2,200	543.45
111,000	1.15	10	–1.2	100	2,200	–1,840.32
111,000	3.15	10	–1.2	–5,100	2,700	–7,615.33
111,000	–0.85	10	–1.1	4,400	2,000	3,097.78
111,000	–1.85	10	–1.1	6,500	1,800	5,429.99

Table B1. Continued.

Vertical load, lb	Slip angle, deg	Speed, KGS	Bank angle, deg	Side force, lb	Drag force, lb	Corrected side load for conicity, lb
			EAFB			
111,000	–2.85	10	–1.1	9,000	1,800	8206.44
111,000	–4.65	10	–1.1	13,200	2,000	12,870.87
127,000	0.05	10	–0.6	1,700	1,500	798.75
127,000	1.15	10	–0.6	–200	1,500	–1,341.63
127,000	3.15	10	–0.6	–5,300	1,800	–7,086.87
127,000	–0.85	10	–0.3	2,900	1,400	2,708.74
127,000	–1.85	10	–0.2	4,600	1,700	4,809.87
127,000	–2.85	10	0.0	7,100	1,900	7,998.27
127,000	–4.85	10	0.0	11,700	2,200	13,180.25
148,000	0.15	10	0.0	300	1,800	344.23
148,000	1.15	10	0.0	–800	1,900	–917.95
148,000	3.15	10	0.0	–5,000	2,400	–5,737.19
148,000	–0.85	10	0.0	2,500	2,300	2,868.59
148,000	–1.85	10	0.0	4,400	2,500	5,048.73
148,000	–2.85	10	0.0	6,400	2,700	7,343.60
148,000	–4.65	10	0.0	10,200	3,200	11,703.86
32,000	0.15	10	0.0	–1,100	200	–1,135.07
32,000	1.15	10	0.0	–4,000	200	–4,127.51
32,000	3.15	10	0.0	–10,300	200	–10,628.35
32,000	6.15	10	0.1	–15,000	200	–15,431.30
32,000	–0.85	10	0.1	1,700	200	1,801.07
32,000	–1.85	10	0.1	4,800	200	4,999.90
32,000	–2.85	10	0.1	7,400	200	7,682.78
32,000	–4.85	10	0.1	11,300	200	11,707.11
32,000	–7.95	10	0.1	13,400	300	13,874.05
47,000	0.25	10	0.1	–1,200	400	–1,187.33
47,000	1.05	10	0.1	–4,700	400	–4,851.21
47,000	3.05	10	0.1	–11,500	500	–11,969.59
47,000	6.05	10	0.1	–18,200	700	–18,983.29
47,000	–0.85	10	0.2	3,000	400	3,278.17

Table B1. Continued.

Vertical load, lb	Slip angle, deg	Speed, KGS	Bank angle, deg	Side force, lb	Drag force, lb	Corrected side load for conicity, lb
			EAFB			
47,000	–1.85	10	0.2	5,300	400	5,685.86
47,000	–2.85	10	0.3	8,100	500	8,685.82
47,000	–4.85	10	0.2	13,800	600	14,583.85
47,000	–7.85	10	0.2	17,900	700	18,875.81
65,000	0.15	10	0.2	–200	700	–22.50
65,000	1.15	10	0.2	–3700	800	–3,749.14
65,000	3.15	10	0.2	–11,100	900	–11,628.31
65,000	6.05	10	0.2	–20,100	1,300	–21,211.09
65,000	–0.85	10	0.3	3,000	800	3,479.93
65,000	–1.85	10	0.3	6,000	800	6,674.19
65,000	–2.95	10	0.3	8,700	900	9,549.03
65,000	–4.95	10	0.4	15,000	1,100	16,352.20
65,000	–7.85	10	0.4	21,200	1,300	22,953.66
80,000	0.15	10	0.5	–500	1,000	46.15
80,000	1.05	10	0.5	–3,200	1,100	–2,869.03
80,000	3.15	10	0.5	–10,300	1,300	–10,534.87
80,000	–1.85	10	0.4	4,500	1,100	5,327.43
80,000	–2.85	10	0.4	8,200	1,200	9,322.31
80,000	–4.75	10	0.4	13,400	1,400	14,936.73
96,000	0.05	10	0.3	–700	600	–345.02
96,000	1.05	10	0.3	–3,300	300	–3,193.68
96,000	3.15	10	0.2	–9,500	700	–10,127.25
96,000	–0.85	10	0.3	2,200	500	2,832.32
96,000	–1.95	10	0.4	4,400	600	5,383.35
96,000	–2.95	10	0.6	7,300	700	8,841.98
96,000	–4.95	10	0.6	13,000	1,200	15,087.10
111,000	0.05	10	0.4	–700	500	–126.94
111,000	1.05	10	0.5	–2,500	500	–1,963.37
111,000	3.15	10	0.4	–8,100	600	–8,345.22
111,000	–0.85	10	0.6	1,500	600	2,641.56

Table B1. Continued.

Vertical load, lb	Slip angle, deg	Speed, KGS	Bank angle, deg	Side force, lb	Drag force, lb	Corrected side load for conicity, lb
			EAFB			
111,000	–2.05	10	0.7	3,800	700	5,358.50
111,000	–2.95	10	0.7	5,600	800	7,357.54
111,000	–4.95	10	0.7	11,800	1,300	14,243.13
127,000	0.05	10	0.7	–1,300	1,500	–162.09
127,000	1.25	10	0.4	–2,300	1,500	–1,846.77
127,000	3.15	10	0.3	–6,800	1,700	–7,102.15
127,000	–0.95	10	0.2	1,700	1,400	2,287.19
127,000	–1.85	10	0.1	4,200	1,600	4,917.43
127,000	–2.85	10	0.0	6,900	1,800	7,772.97
127,000	–4.95	10	0.0	11,900	2,200	13,405.56
148,000	0.15	10	0.0	300	1,800	344.23
148,000	1.15	10	0.0	–600	1,600	–688.46
148,000	3.15	10	0.0	–4,800	2,200	–5,507.70
148,000	–0.85	10	0.0	1,700	1,800	1,950.64
148,000	–1.85	10	0.0	3,800	1,800	4,360.26
148,000	–2.85	10	0.0	5,900	1,900	6,769.88
148,000	–4.95	10	0.0	10,500	2,700	12,048.09
			KSC			
62,000	–5.4	193	2.5	14,400	2,300	17,560.16
66,500	–5.3	136	0.1	15,500	2,500	16,624.26
62,200	–3.3	148	–0.3	10,900	1,200	11,302.03
91,900	–2.4	145	0.1	6,000	1,700	6,683.94
62,100	–2.3	147	0.1	7,600	700	8,161.14
62,000	–2.3	139	0.3	7,100	800	7,811.02
46,300	–2.4	145	0.1	8,300	300	8,750.66
62,300	–3.4	150	0.2	11,500	700	12,396.27
62,400	–2.4	154	0.7	8,100	700	9,243.43
61,500	–0.3	100	0.2	800	600	1,029.21
122,200	0.9	52	–1.4	900	2,000	–1,496.76
122,200	2.1	52	–1.6	–1,400	2,000	–4,434.80

Table B1. Concluded.

Vertical load, lb	Slip angle, deg	Speed, KGS	Bank angle, deg	Side force, lb	Drag force, lb	Corrected side load for conicity, lb
KSC						
122,200	3.9	52	–1.6	–4,700	2,500	–8,136.53
91,700	–1.3	52	–1.2	4,500	1,000	3,299.00
91,700	–2.0	52	–1.0	6,800	1,100	6,077.79
91,700	–4.0	52	–0.9	12,100	1,400	11,996.29
91,700	–7.0	52	–0.8	18,800	2,200	19,442.68
61,500	0.8	52	–1.4	1,200	600	12.15
61,500	1.7	52	–1.1	–3,000	600	–4,174.87
61,500	3.7	52	–0.7	–9,400	700	–10,606.59
61,500	6.5	52	–0.7	–18,600	1,100	–20,370.24
46,100	–1.0	52	–0.3	1,600	300	1,470.87
46,100	–1.9	52	–0.7	5,700	300	5,489.02
46,100	–3.9	52	–0.8	11,300	300	11,278.66
46,100	–7.0	52	–0.6	17,600	500	18,003.06
46,700	–2.3	104	0.3	7,800	300	8,368.12
122,700	0.6	152	–0.1	200	2,000	44.69
122,700	1.5	152	–0.2	–1,200	2,000	–1,706.19
122,700	3.7	152	–0.4	–6,500	2,500	–8,013.54
92,100	–1.4	154	0.4	3,600	1,100	4,470.01
92,100	–2.3	154	0.6	4,900	1,100	6,159.13
92,100	–4.1	154	0.3	9,800	1,300	11,103.93
92,100	–7.3	154	0.6	18,800	3,500	21,334.46
61,500	0.7	159	0.4	–1,600	400	–1,337.64
61,500	1.7	159	0.3	–5,000	500	–5,036.04
61,500	3.6	159	0.4	–9,700	500	–9,933.89
61,500	6.5	159	0.4	–17,500	800	–18,211.77
46,900	–1.4	160	0.5	4,000	200	4,530.43
46,900	–2.4	160	0.7	6,400	200	7,179.98
46,900	–4.2	160	0.6	10,800	300	11,716.85
46,900	–7.2	160	0.7	16,100	500	17,333.18

Table B2. Data from nose tire dry concrete tire force tests.

Vertical load, lb	Slip angle, deg	Speed, KGS	Bank angle, deg	Side force, lb	Drag force, lb	Corrected side load for conicity, lb
EAFB						
50,000	0.0	199	0.4	–100	1,700	188.02
50,000	1.1	199	0.3	–600	1,200	–410.14
50,000	2.2	199	0.2	–1,300	1,500	–1,218.25
50,000	4.1	199	–0.1	–2,500	1,800	–2,697.78
50,000	7.2	199	–0.4	–5,200	2,000	–5,752.01
50,000	0.2	199	–0.3	400	1,600	200.17
50,000	–0.8	199	–0.2	800	1,400	693.35
50,000	–1.8	199	0.0	1,700	1,200	1,784.68
50,000	–3.8	199	0.1	2,400	1,800	2,592.79
32,000	0.0	50	0.1	–500	300	–469.06
32,000	1.0	50	0.1	–2,000	400	–2,016.88
32,000	2.0	50	0.1	–3,900	400	–3,977.45
32,000	4.0	50	0.1	–6,600	500	–6,763.52
32,000	0.0	50	0.1	–600	300	–572.25
32,000	–1.0	50	0.1	1,100	400	1,181.95
32,000	–2.0	50	0.1	2,200	400	2,317.01
32,000	–3.9	50	0.1	4,800	400	4,999.90
12,000	0.0	50	–0.1	–400	100	–422.36
12,000	1.0	50	–0.1	–1,500	100	–1,535.51
12,000	2.0	50	–0.1	–2,500	100	–2,547.47
12,000	4.0	50	–0.1	–4,000	100	–4,065.40
12,000	0.0	50	–0.1	–500	100	–523.56
12,000	–1.0	50	–0.1	700	100	690.79
12,000	–2.0	50	–0.1	1,600	100	1,601.55
12,000	–4.0	50	–0.1	3,100	100	3,119.48
31,000	0.0	160	0.3	–200	800	–69.93
31,000	1.0	160	0.3	–2,200	800	–2,131.70
31,000	2.0	160	0.3	–3,800	800	–3,781.11
31,000	4.0	160	0.2	–6,500	800	–6,609.90

Table B2. Concluded.

Vertical load, lb	Slip angle, deg	Speed, KGS	Bank angle, deg	Side force, lb	Drag force, lb	Corrected side load for conicity, lb
			EAFB			
31,000	0.0	160	0.1	–800	700	–779.29
31,000	–1.0	160	0.1	500	700	560.86
31,000	–2.0	160	0.1	2,200	700	2,313.36
31,000	– 4.0	160	0.1	4,700	700	4,890.56
11,000	0.0	160	0.0	–300	500	–303.29
11,000	1.0	160	0.0	–1,600	500	–1,617.53
11,000	2.0	160	0.0	–2,300	500	–2,325.20
11,000	4.0	160	0.0	– 4,300	500	– 4,347.12
11,000	0.0	160	0.0	–500	400	–505.48
11,000	–1.0	160	0.0	600	400	606.57
11,000	–2.1	160	0.0	1,400	400	1,415.34
11,000	– 4.0	160	0.0	3,100	500	3,133.97
30,000	0.0	199	0.0	0	1,000	0.00
30,000	1.0	199	–0.1	–2,200	1,000	–2,309.70
30,000	2.0	199	–0.2	–3,600	1,000	–3,795.49
30,000	4.0	199	–0.4	–6,500	1,000	–6,870.06
30,000	0.0	199	–0.4	–100	1,000	–278.79
30,000	–1.0	199	–0.3	1,400	1,000	1,309.99
30,000	–2.0	199	–0.1	2,900	1,000	2,942.72
30,000	– 4.0	199	0.1	5,000	1,000	5,193.38
12,000	0.0	200	0.3	–400	600	–352.04
12,000	1.0	200	0.3	–1,600	600	–1,566.39
12,000	2.0	200	0.3	–2,200	600	–2,173.56
12,000	4.0	200	0.3	– 4,400	600	– 4,399.86
12,000	0.0	200	0.2	–600	700	–572.01
12,000	–1.0	200	0.2	400	700	439.94
12,000	–2.0	200	0.2	1,600	700	1,654.29
12,000	– 4.0	200	0.2	3,400	700	3,475.80

Table B3. Data from main tire lakebed tire force tests.

Vertical load, lb	Slip angle, deg	Speed, KGS	Bank angle, deg	Side force, lb	Drag force, lb	Corrected side load for conicity, lb
			EAFB			
124,000	1.1	51	–1.7	3,600	4,700	956.48
124,000	2.6	51	–1.3	1,300	4,700	–900.99
124,000	4.4	51	–1.5	–800	4,300	–3,623.72
124,000	6.6	51	–1.6	–4,500	4,600	–7,962.44
91,000	0.5	50	–0.2	500	3,200	278.70
91,000	–0.5	50	–0.4	1,600	3,300	1,211.79
91,000	–1.5	50	–0.6	4,800	3,700	4,435.25
91,000	–3.5	50	–0.6	11,100	4,000	11,306.37
91,000	–6.5	50	–0.6	18,900	4,600	19,813.47
61,000	0.3	48	–0.3	1,600	2,300	1,429.13
61,000	1.2	48	–0.2	700	2,500	563.81
61,000	2.3	48	0.1	–4,700	2,500	–4,896.25
61,000	4.4	48	0.2	–11,300	2,800	–11,807.95
61,000	7.4	48	0.0	–20,000	3,100	–21,215.36
47,000	0.5	48	0.4	–1,500	1,700	–1,294.81
47,000	–0.5	48	0.3	1,200	1,400	1,462.75
47,000	–1.4	48	0.2	4,400	1,500	4,743.72
47,000	–3.5	48	0.2	10,300	1,800	10,919.97
47,000	–6.6	48	0.4	16,600	1,900	17,652.66
123,000	1.1	159	–1.8	2,500	8,100	–437.18
123,000	2.0	159	–1.7	–100	8,100	–3,175.57
123,000	2.9	159	–1.8	–2,200	8,700	–5,713.08
123,000	4.7	159	–1.8	–7,000	9,700	–11,101.24
92,000	0.3	153	–1.3	2,000	6,900	431.16
92,000	0.8	153	–1.1	1,300	6,300	–63.43
92,000	0.0	153	–1.0	2,100	6,300	944.67
92,000	–0.8	153	–1.0	3,200	6,300	2,145.48
92,000	–2.6	153	–0.9	9,500	6,400	9,157.66
92,000	–5.7	153	–0.8	17,800	7,100	18,353.14
61,000	0.8	156	–0.5	500	4,100	83.56
61,000	1.3	156	–0.4	–1,900	4,400	–2,372.92
61,000	2.4	156	–0.3	–5,400	4,600	–5,996.24
61000	4.5	156	–0.4	–11,700	4,800	–12,768.45

Table B4. Data from nose tire lakebed tire force tests.

Vertical load, lb	Slip angle, deg	Speed, KGS	Bank angle, deg	Side force, lb	Drag force, lb	Corrected side load for conicity, lb
			EAFB			
61,000	7.5	156	–0.7	–18,800	5,100	–20,568.00
47,000	–0.1	160	0.0	100	3,700	104.68
47,000	–0.1	160	–0.1	500	3,700	454.56
47,000	–0.4	160	–0.2	1,500	3,300	1,432.52
47,000	–2.2	160	–0.1	7,600	3,400	7,886.99
47,000	–5.7	160	0.0	14,700	3,600	15,388.27
126,000	0.5	192	–1.5	3,200	8,000	832.82
126,000	1.3	192	–1.3	900	8,000	–1,386.70
126,000	1.9	192	–1.4	–1,900	8,200	–4,722.75
126,000	3.7	192	–1.3	–5,500	8,500	–8,590.04
92,000	0.4	186	–0.3	400	6,100	32.32
92,000	–0.4	186	–0.3	2,100	6,100	1,888.13
92,000	–1.4	186	–0.3	5,500	6,300	5,599.74
92,000	–3.6	186	–0.3	11,600	6,500	12,258.80
92,000	–6.5	186	–0.2	18,800	7,600	20,253.47
62,000	1.3	185	–0.1	–1,100	4,200	–1,258.77
62,000	1.3	185	0.1	–1,900	4,200	–1,926.52
62,000	1.8	185	0.4	–4,700	4,400	–4,626.97
62,000	3.4	185	0.3	–9,000	4,700	–9,283.39
62,000	6.1	185	0.1	–16,600	5,000	–17,534.46
47,000	–0.1	185	0.6	–700	3,300	–319.64
47,000	0.1	185	0.3	400	3,300	625.29
47,000	–1.0	185	0.4	3,400	3,500	3,834.61
47,000	–3.5	185	0.5	9,800	3,800	10,603.12
11,000	0.3	50	0.8	–100	200	27.82
11,000	1.3	50	0.8	–1,400	200	–1,286.42
11,000	2.3	50	0.8	–2,100	200	–1,994.09
11,000	4.3	50	0.8	–4,000	200	–3,914.91
11,000	0.3	50	0.8	–300	100	–174.37
11,000	–0.7	50	0.8	900	100	1,038.78
11,000	–1.7	50	0.8	1,600	100	1,746.45
11,000	–3.7	50	0.8	3,200	100	3,363.99
31,000	–0.4	162	–0.3	400	2,000	276.11

Table B4. Concluded.

Vertical load, lb	Slip angle, deg	Speed, KGS	Bank angle, deg	Side force, lb	Drag force, lb	Corrected side load for conicity, lb
			EAFB			
31,000	0.7	162	–0.3	–900	2,000	–1,064.04
31,000	1.6	162	–0.3	–1,800	2,000	–1,991.83
31,000	3.7	162	–0.3	–4,600	2,000	–4,878.30
31,000	–0.3	162	–0.3	500	2,000	379.20
31,000	–1.3	162	–0.3	1,700	2,000	1,616.25
31,000	–2.3	162	–0.3	3,000	2,000	2,956.40
31,000	–4.3	162	–0.3	5,400	2,000	5,430.52
11,000	–0.4	161	0.1	300	900	319.40
11,000	0.7	161	0.1	–1,500	900	–1,500.32
11,000	1.8	161	–0.2	–2,000	900	–2,054.15
11,000	3.8	161	–0.3	–2,500	900	–2,575.74
11,000	–0.4	161	–0.2	700	900	675.44
11,000	–1.4	161	–0.2	1,500	900	1,484.21
11,000	–2.5	161	0.0	2,200	900	2,224.11
11,000	–4.4	161	0.0	3,500	900	3,538.35
31,000	–0.1	201	0.6	200	2,100	478.67
31,000	1.1	201	–0.6	–700	2,100	–994.11
31,000	2.0	201	–0.6	–1,700	2,100	–2,024.99
31,000	3.8	201	–0.6	–4,000	2,100	–4,396.02
31,000	–0.1	201	–0.7	200	2,200	–111.73
31,000	0.9	201	–0.6	1,300	2,200	1,067.66
31,000	–1.7	201	–0.6	2,500	2,200	2,304.72
31,000	–3.7	201	–0.5	4,700	2,200	4,618.07
12,000	–0.2	201	–0.3	200	1,100	149.65
12,000	0.7	201	–0.3	–700	1,100	–761.11
12,000	1.7	201	–0.3	–1,300	1,100	–1,368.28
12,000	3.7	201	–0.3	–2,700	1,100	–2,785.01
12,000	–0.3	201	–0.2	200	1,100	167.23
12,000	–1.1	201	–0.2	1,100	1,100	1,077.99
12,000	–2.0	201	–0.2	1,900	1,100	1,887.55
12,000	–3.7	201	–0.2	3,200	1,100	3,203.09

Table B5. Data from main tire wet runway tire force tests.

Vertical load, lb	Rotopeen or skid abrade	Slip angle, deg	Speed, KGS	Bank angle, deg	Side force, lb	Corrected side load for conicity, lb
			KSC			
124,000	rot2	1.0	153	–0.1	–100	–294.01
124,000	rot2	2.0	153	–0.2	–3,000	–3,733.91
124,000	rot2	4.0	153	–0.3	–7,700	–9,196.15
93,000	rot2	–1.0	157	0.2	3,300	3,878.22
93,000	rot2	–1.9	157	0.3	4,900	5,762.70
93,000	rot2	–3.9	157	0.2	11,100	12,400.87
93,000	rot2	–6.9	157	0.3	17,400	19,420.79
63,000	rot2	1.2	159	–0.2	–3,600	–4,010.53
63,000	rot2	2.0	159	–0.1	–5,000	–5,406.10
63,000	rot2	3.9	159	0.0	–10,000	–10,627.61
63,000	rot2	7.1	159	–0.2	–15,800	–16,976.21
47,000	rot2	–1.0	159	0.0	2,900	3,035.78
47,000	rot2	–1.9	159	0.1	5,200	5,512.33
47,000	rot2	–3.9	159	0.0	9,300	9,735.44
47,000	rot2	–7.0	159	0.1	12,300	12,944.76
56,000	skid1	1.1	203	–0.8	–1,200	–1,923.26
60,000	skid1	2.6	203	–1.7	–2,600	–4,249.71
36,000	skid1	0.6	203	–1.4	–1,900	–2,706.50
124,000	skid1	1.0	52	–0.3	–1,300	–2,005.57
124,000	skid1	2.0	52	–0.5	–4,300	–5,739.47
124,000	skid1	4.0	52	–0.8	–7,800	–10,216.80
92,000	skid1	–0.8	52	–0.7	1,900	1,130.68
92,000	skid1	–1.8	52	–0.3	4,600	4,617.25
92,000	skid1	–3.9	52	–0.2	8,500	9,009.47
92,000	skid1	–6.9	52	–0.1	12,400	13,401.68
62,000	rot2	1.0	50	0.0	–3,800	–4,034.70
62,000	rot2	2.0	50	–0.2	–7,400	–8,038.72
62,000	rot2	4.2	50	–0.4	–10,400	–11,405.67
62,000	rot2	7.0	50	–0.1	–12,600	–13,469.06
47,000	skid1	–0.8	50	–0.3	1,400	1,258.98

Table B5. Concluded.

Vertical load, lb	Rotopeen or skid abrade	Slip angle, deg	Speed, KGS	Bank angle, deg	Side force, lb	Corrected side load for conicity, lb
			KSC			
47,000	skid1	–1.9	50	–0.1	3,700	3,804.38
47,000	skid1	–3.9	50	–0.1	7,200	7,468.26
47,000	skid1	–6.8	50	–0.1	9,200	9,561.90
124,000	rot2	1.2	50	–0.3	0	–544.98
124,000	rot2	2.0	50	–0.7	–2,200	–3,743.38
124,000	rot2	4.0	50	–0.8	–7,100	–9,430.33
92,000	rot2	–0.8	51	–0.6	3,300	2,793.77
92,000	rot2	–1.9	51	0.1	6,000	6,684.68
92,000	rot2	–3.9	51	0.1	11,500	12,688.76
92,000	rot2	–6.8	51	0.0	18,200	19,868.04
62,000	rot2	1.0	50	0.3	–1,900	–1,744.86
62,000	rot2	2.0	50	0.2	–6,700	–6,932.16
62,000	rot2	4.2	50	–0.4	–12,300	–13,423.02
62,000	rot2	7.1	50	–0.3	–17,500	–18,853.37
46,000	rot2	–0.9	50	–0.4	3,000	2,867.92
46,000	rot2	–2.0	50	0.0	6,700	7,007.03
46,000	rot2	–3.9	50	0.0	10,800	11,294.91
46,000	rot2	–7.0	50	0.0	14,500	15,164.47
59,000	rot2	1.1	195	0.8	–2,200	–1,637.83
48,000	skid1	1.9	195	0.8	–2,900	–2,476.11
48,000	skid1	4.0	195	0.6	–4,600	–4,398.04
48,000	skid1	7.2	195	0.5	–4,600	–4,468.36
62,000	skid1	–1.0	195	1.0	3,300	4,412.12
62,000	skid1	–1.9	195	1.2	4,900	6,292.61
62,000	skid1	–3.9	195	1.5	10,200	12,192.45
62,000	skid1	–7.0	195	1.9	13,300	15,847.24

REFERENCES

[1]Carter, John F. and Christopher J. Nagy, *The NASA Landing Gear Test Airplane*, NASA TM-4703, 1995.

[2]Davis, Pamela A., Sandy M. Stubbs, and John A. Tanner, *Aircraft Landing Dynamics Facility: A Unique Facility With New Capabilities*, SAE Technical Paper Series 851938, Oct. 1985.

[3]Daugherty, Robert H., Sandy M. Stubbs, and Martha P. Robinson, *Cornering Characteristics of the Main-Gear Tire of the Space Shuttle Orbiter*, NASA TP-2790, 1988.

[4]Vogler, William A. and John A. Tanner, *Cornering Characteristics of the Nose-Gear Tire of the Space Shuttle Orbiter*, NASA TP-1917, 1981.

[5]Daugherty, Robert H. and Thomas J. Yager, *Texture Modification of the Shuttle Landing Facility Runway at the NASA Kennedy Space Center*, NASA TM-110269, 1996.

[6]Tanner, John A., Sandy M. Stubbs, and John L. McCarty, *Static and Yawed-Rolling Mechanical Properties of Two Type VII Aircraft Tires*, NASA TP-1863, 1981.

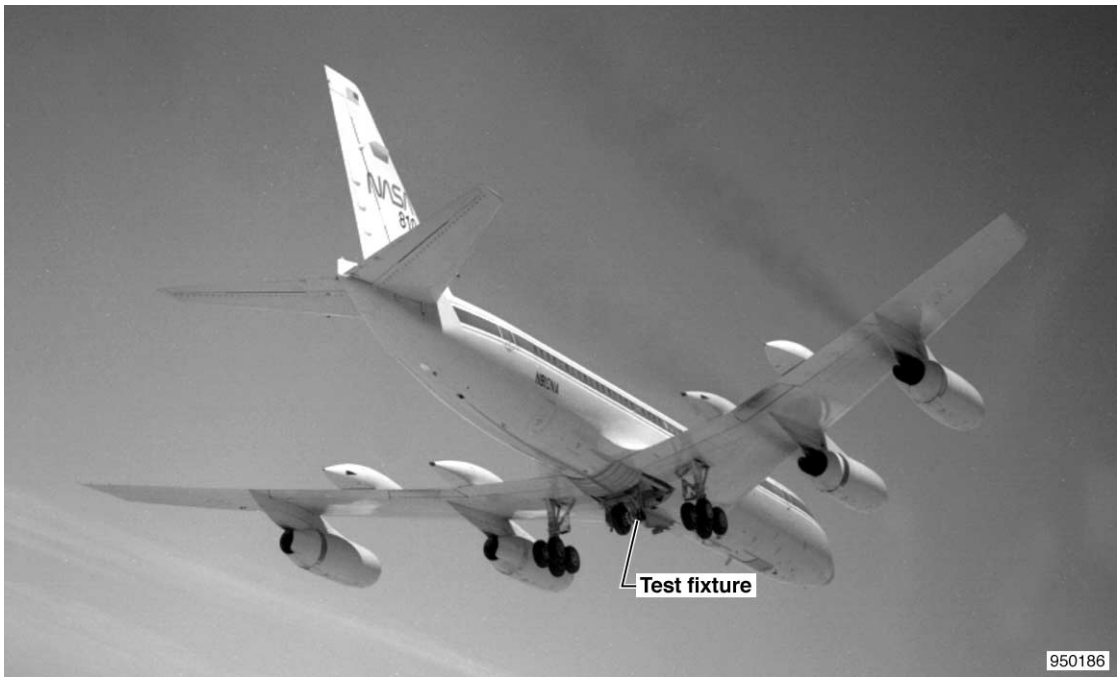

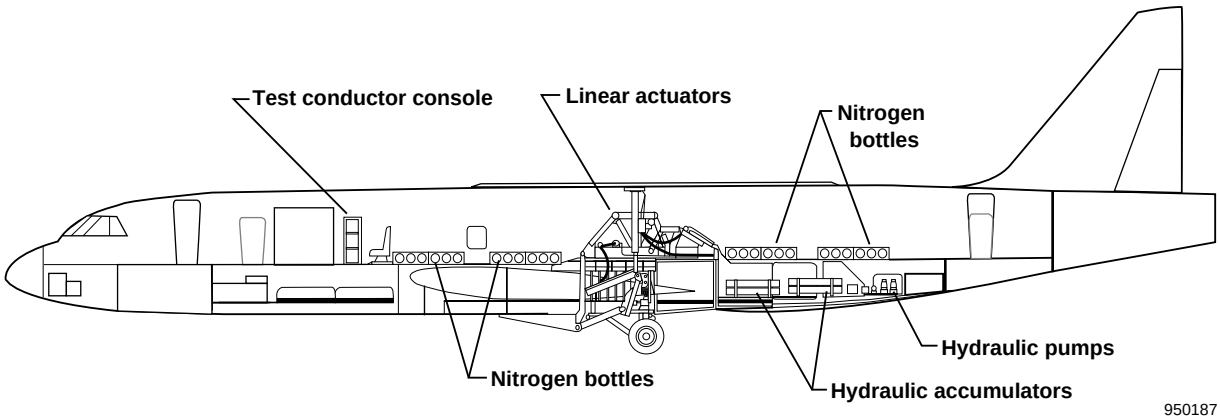

Figure 1. The primary components of the CV 990 aircraft and test system.

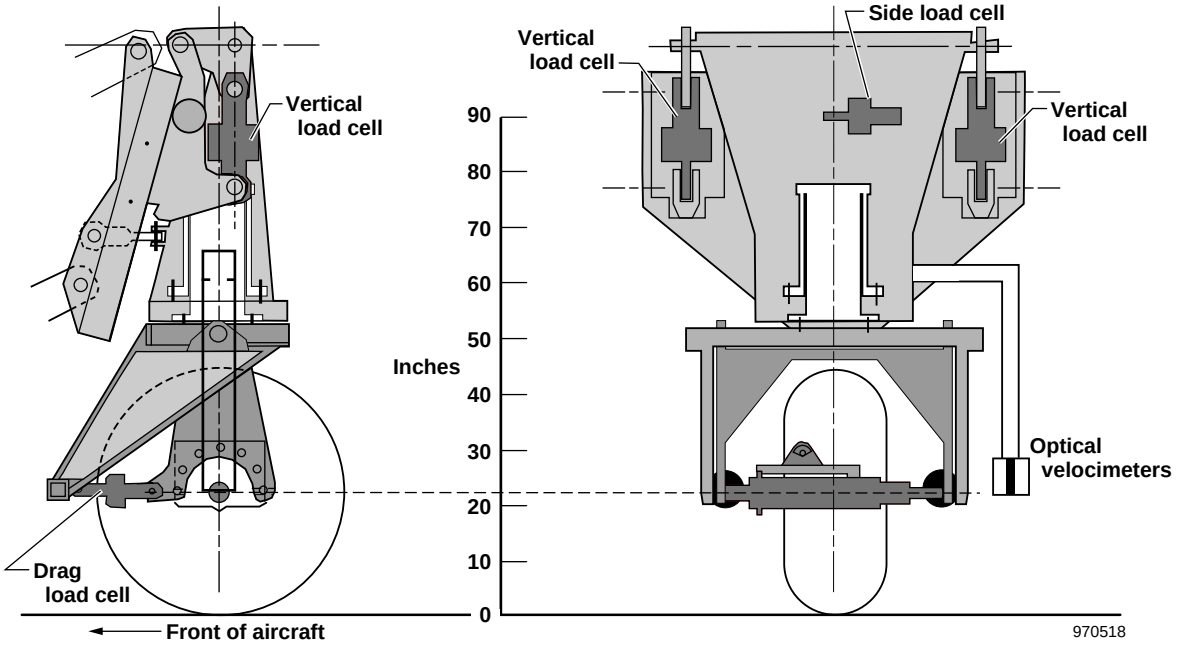

Figure 2. Yaw fixture load cell installation.

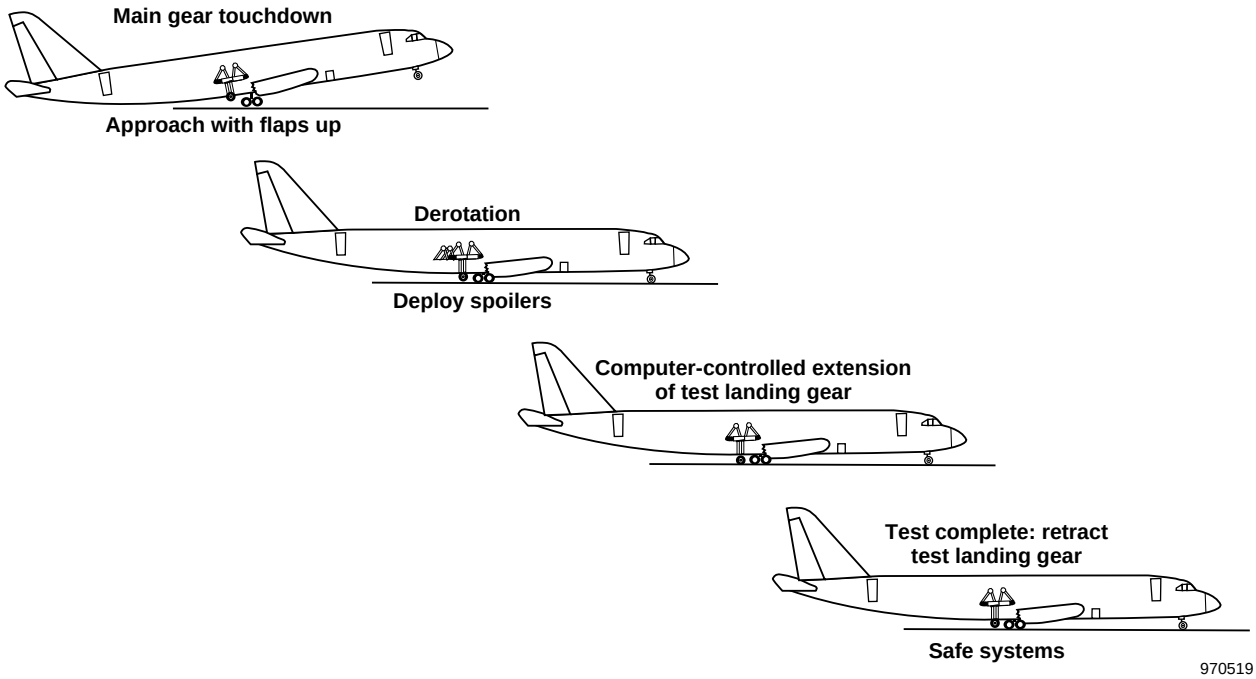

Figure 3. Typical landing sequence.

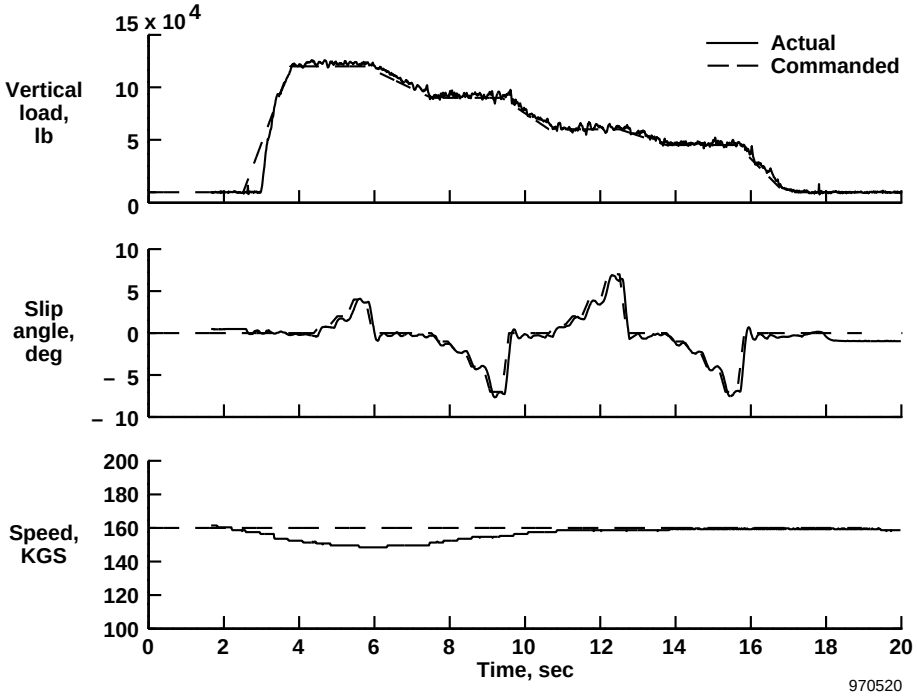

Figure 4. Commanded versus actual tire force data.

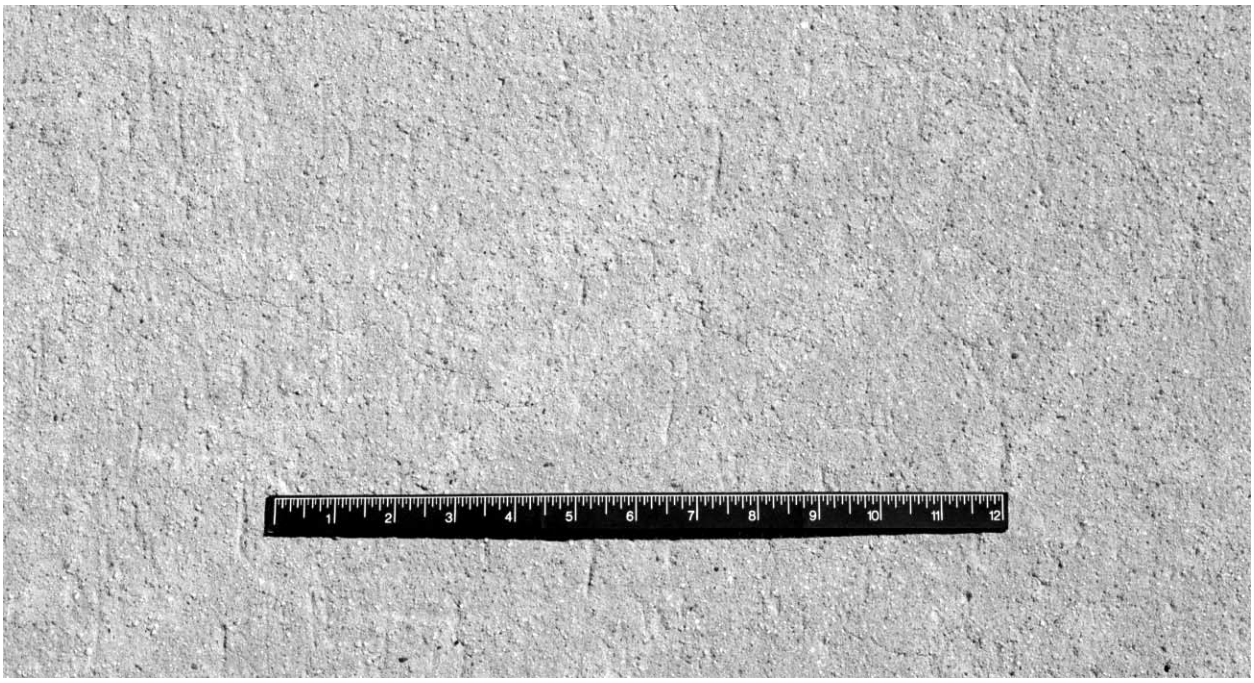

EC97 44019-01

(a) The EAFB concrete runway 22.

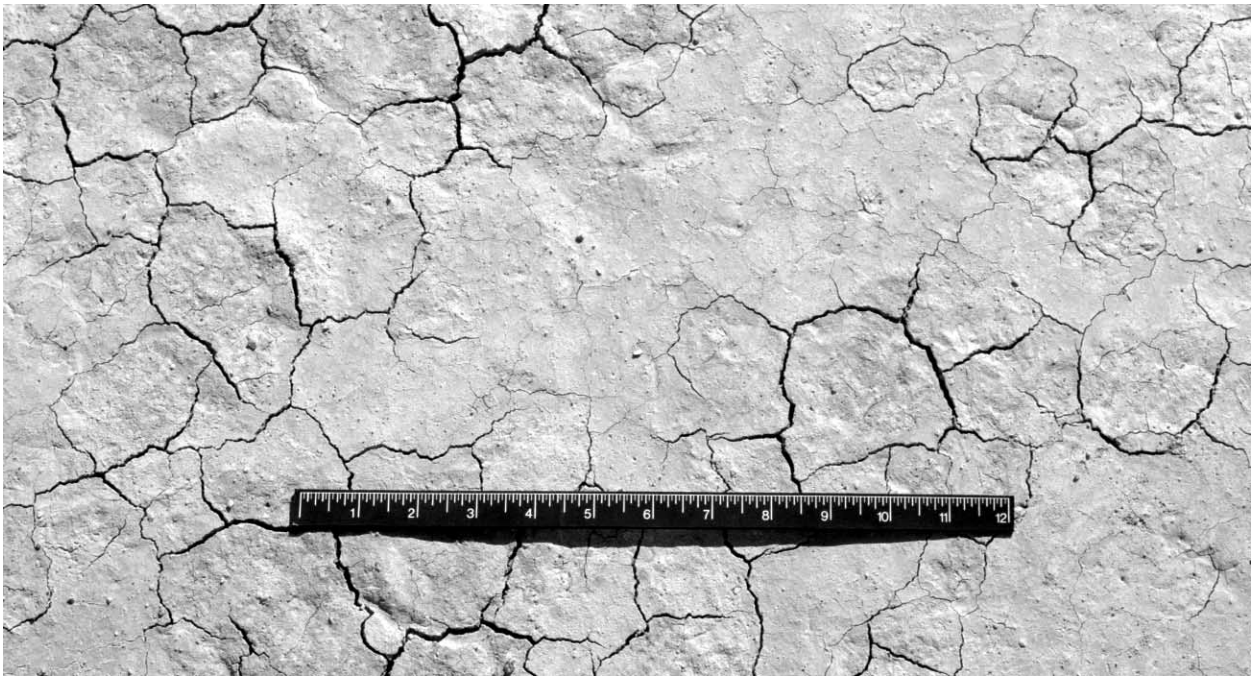

EC97 44019-02

(b) The EAFB lakebed runway 15.

Figure 5. The EAFB surfaces used for tire force testing.

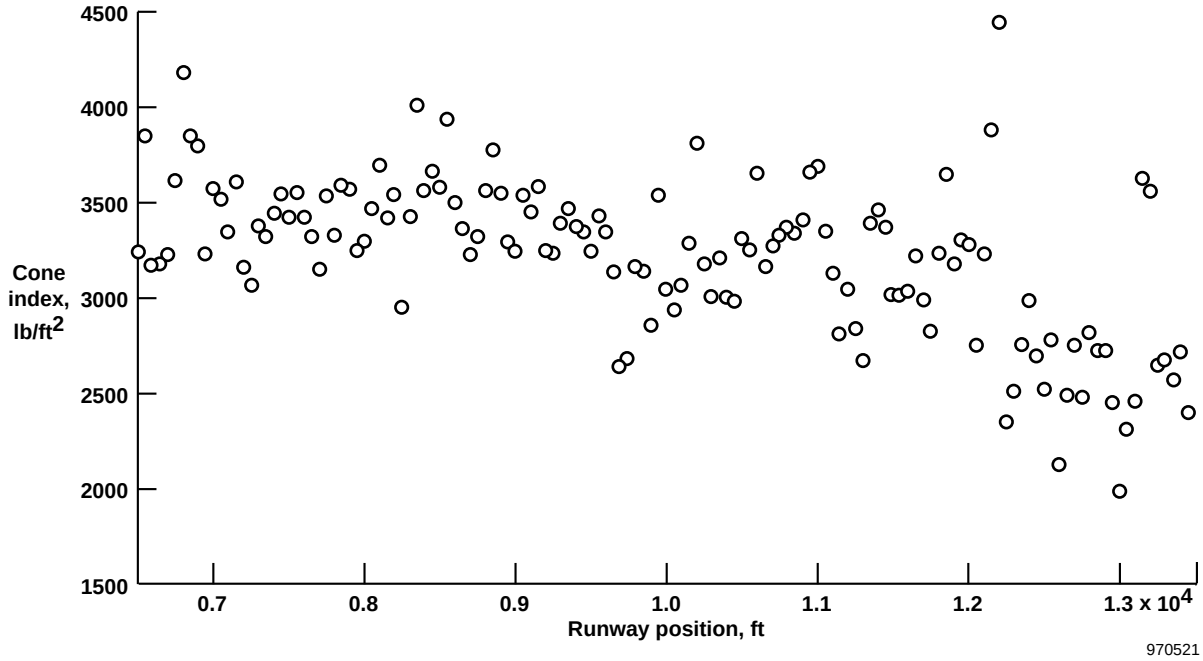

Figure 6. The EAFB runway 15 soil strength: average 0- to 6-in. interval.

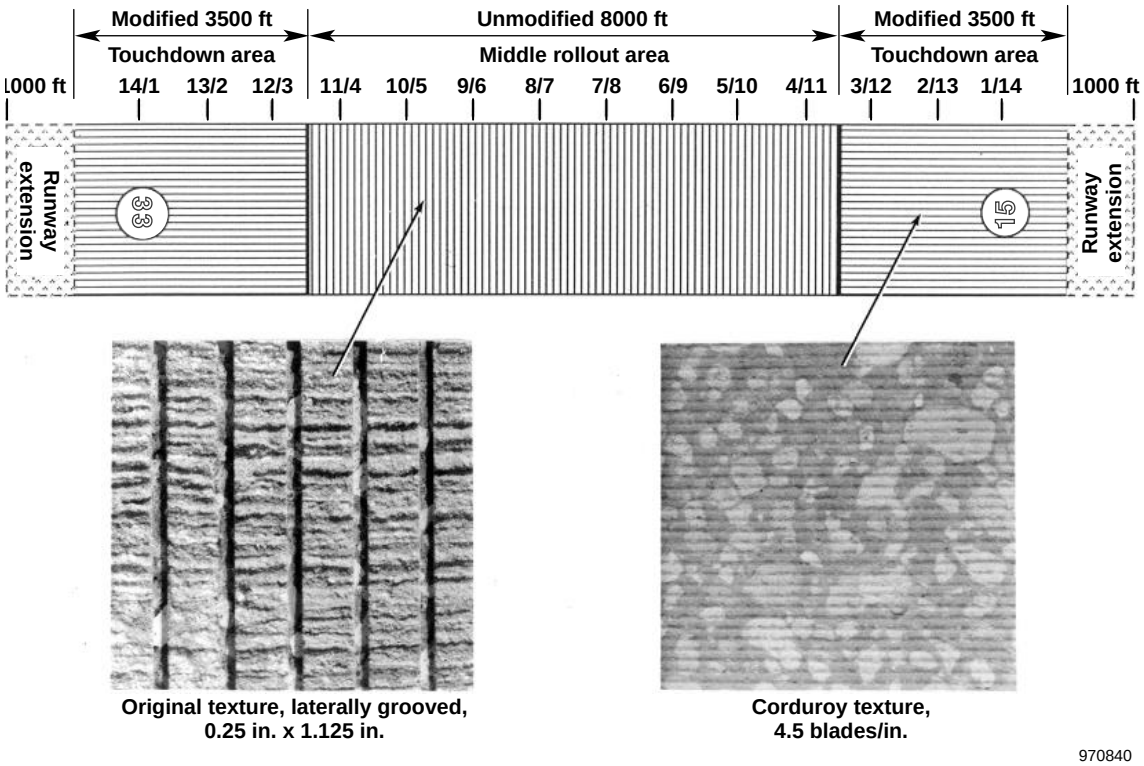

Figure 7. The KSC Shuttle Landing Facility layout (from ref. 5).

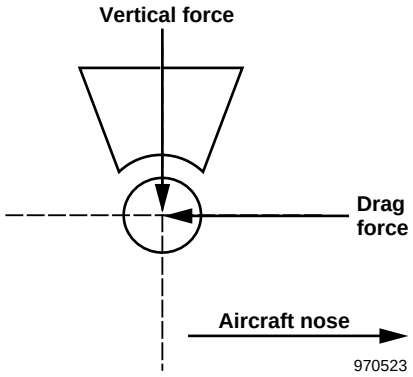

(a) Side view.

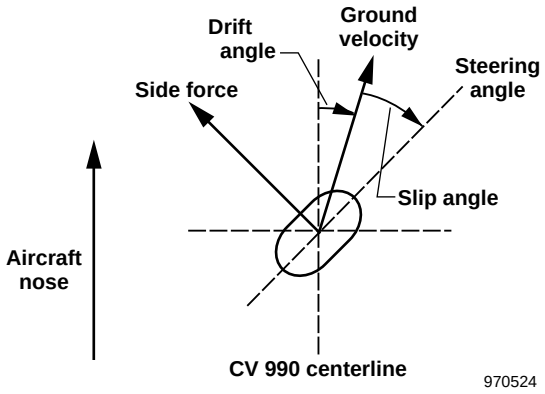

(b) Top view.

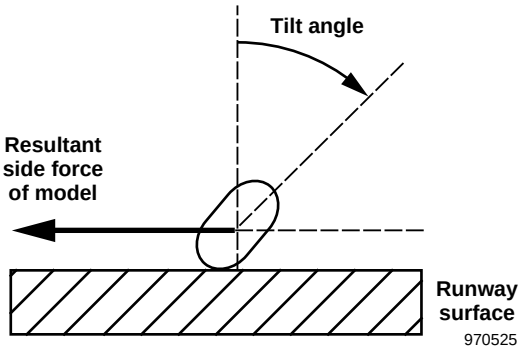

(c) Aft view.

Figure 8. Sign conventions for test tires.

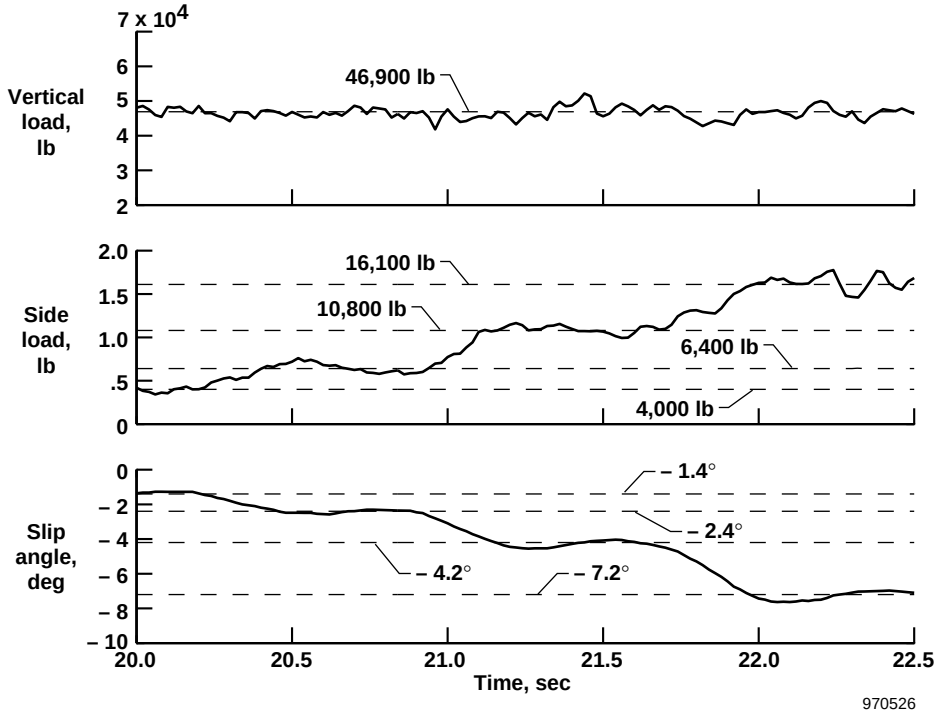

Figure 9. A tire force test on the KSC center section at 160 kn for 2.5 sec.

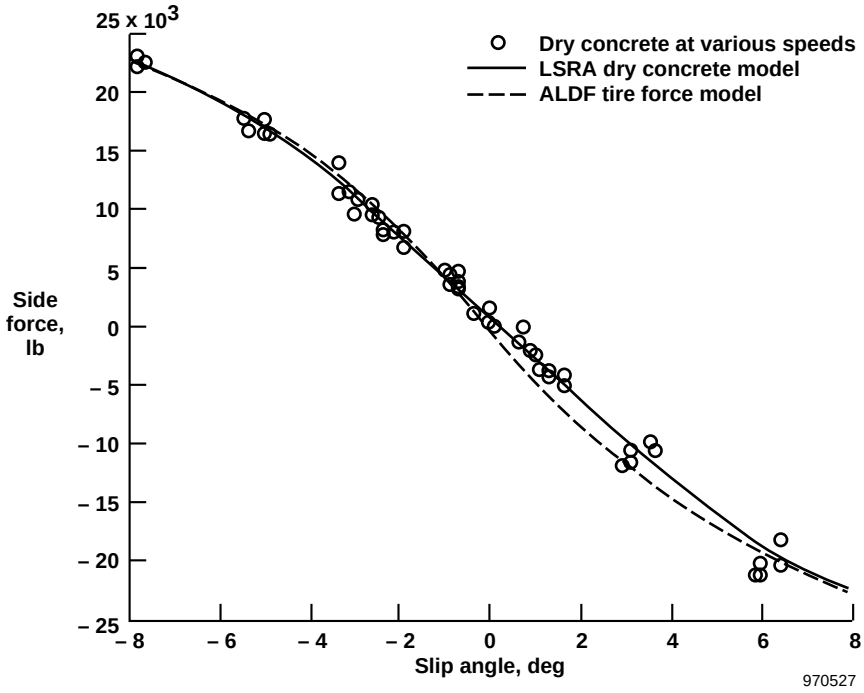

Figure 10. Side force at 63,000 lb ± 2,000 lb with LSRA dry concrete data.

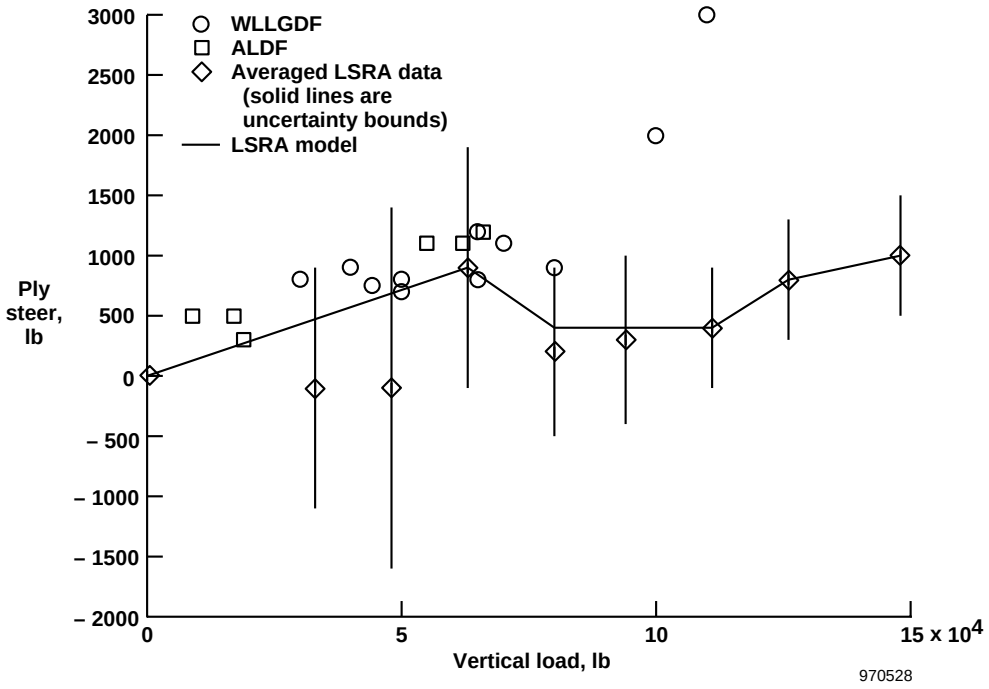

Figure 11. Ply steer estimate.

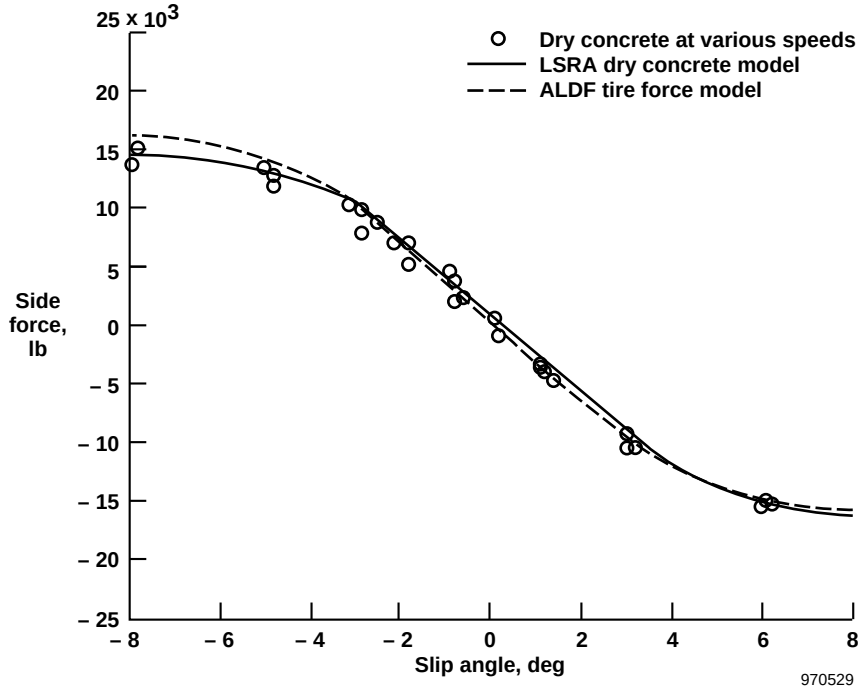

Figure 12. Main gear EAFB and KSC dry concrete side forces at a 33,000-lb vertical load.

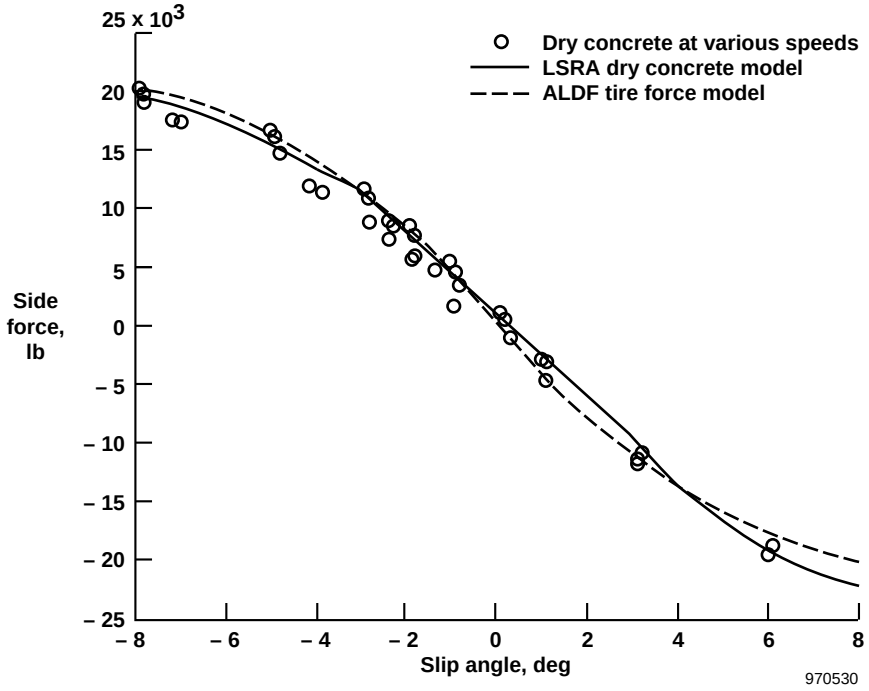

Figure 13. Main gear EAFB and KSC dry concrete side forces at a 48,000-lb vertical load.

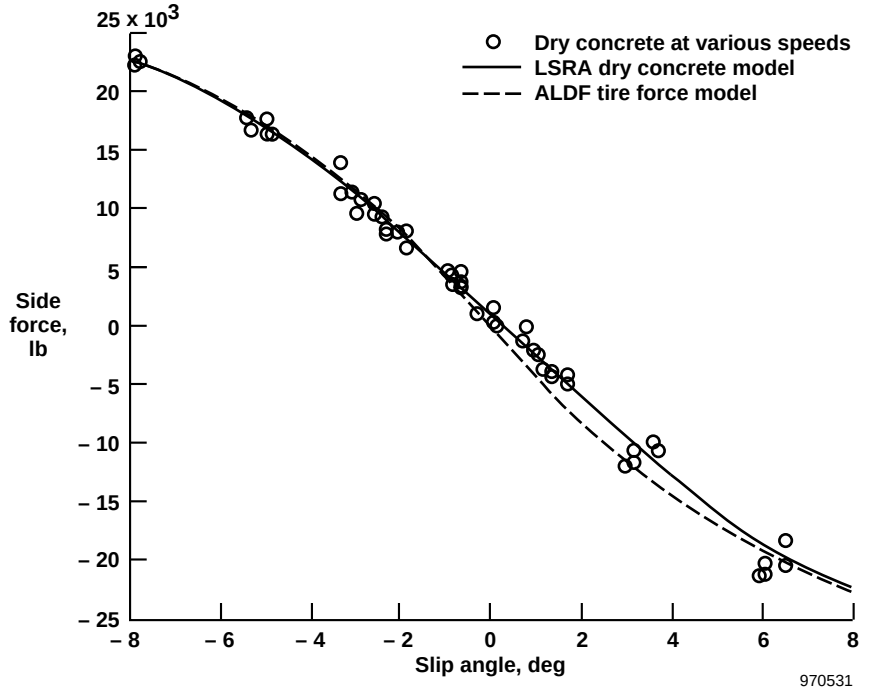

Figure 14. Main gear EAFB and KSC dry concrete side forces at a 63,000-lb vertical load.

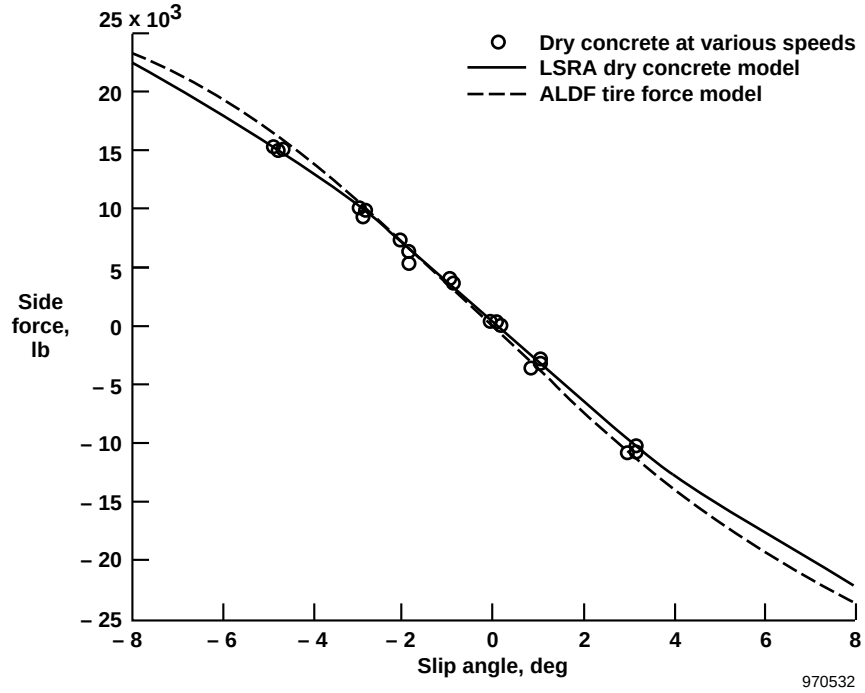

Figure 15. Main gear EAFB and KSC dry concrete side forces at a 80,000-lb vertical load.

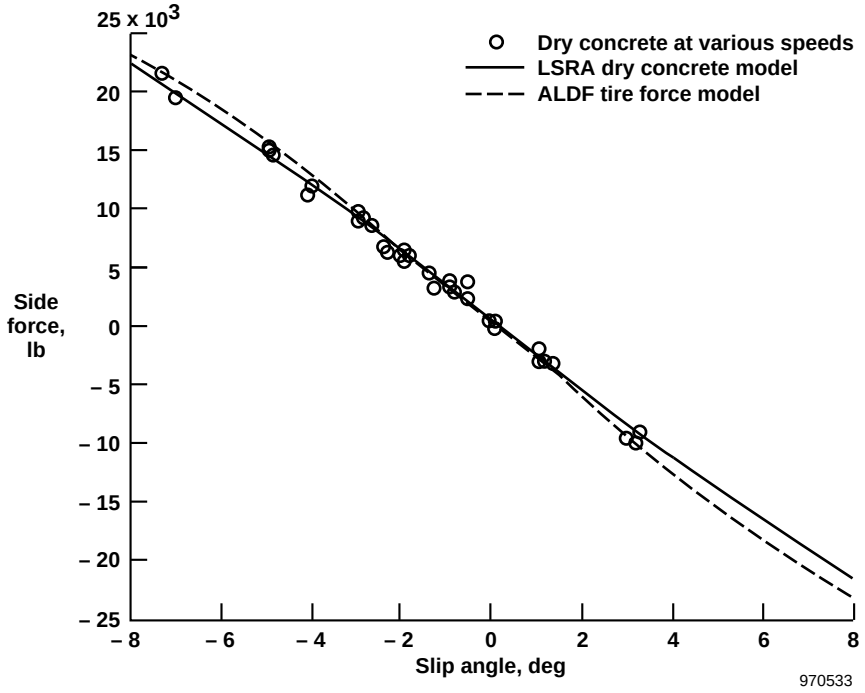

Figure 16. Main gear EAFB and KSC dry concrete side forces at a 94,000-lb vertical load.

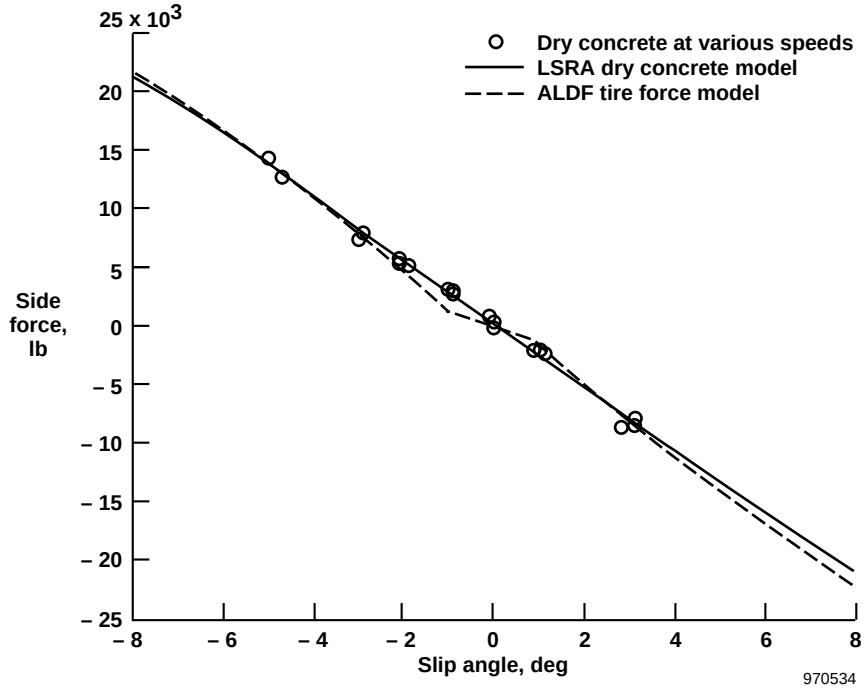

Figure 17. Main gear EAFB and KSC tire dry concrete side forces at a 110,000-lb vertical load.

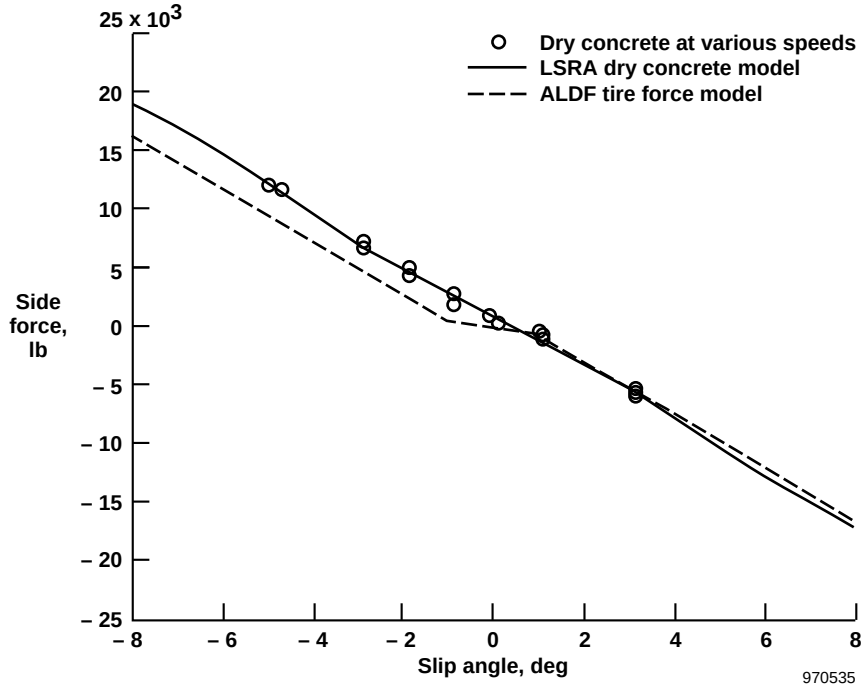

Figure 18. Main gear EAFB and KSC tire dry concrete side forces at a 126,000-lb vertical load.

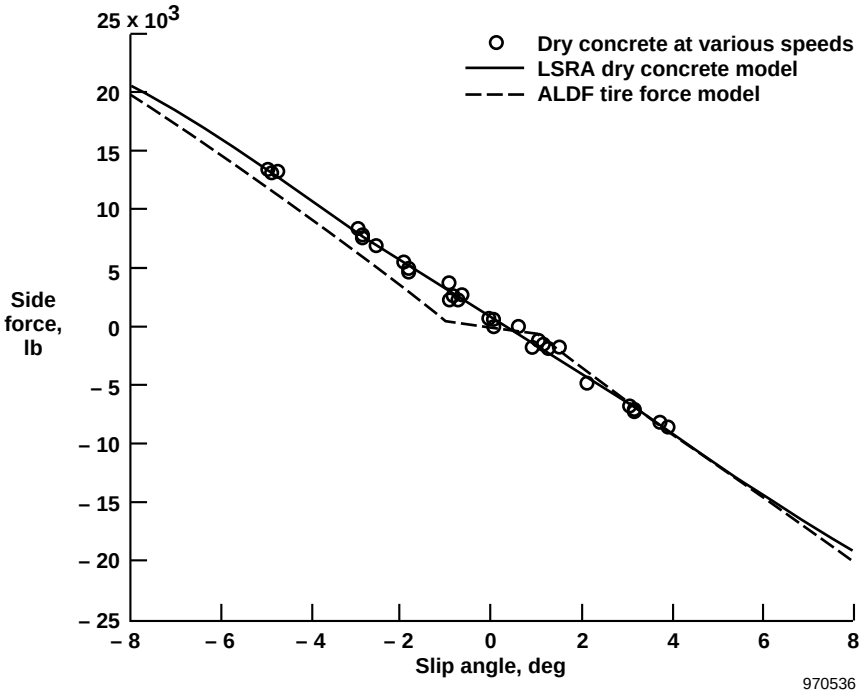

Figure 19. Main gear EAFB and KSC tire dry concrete side forces at a 148,000-lb vertical load.

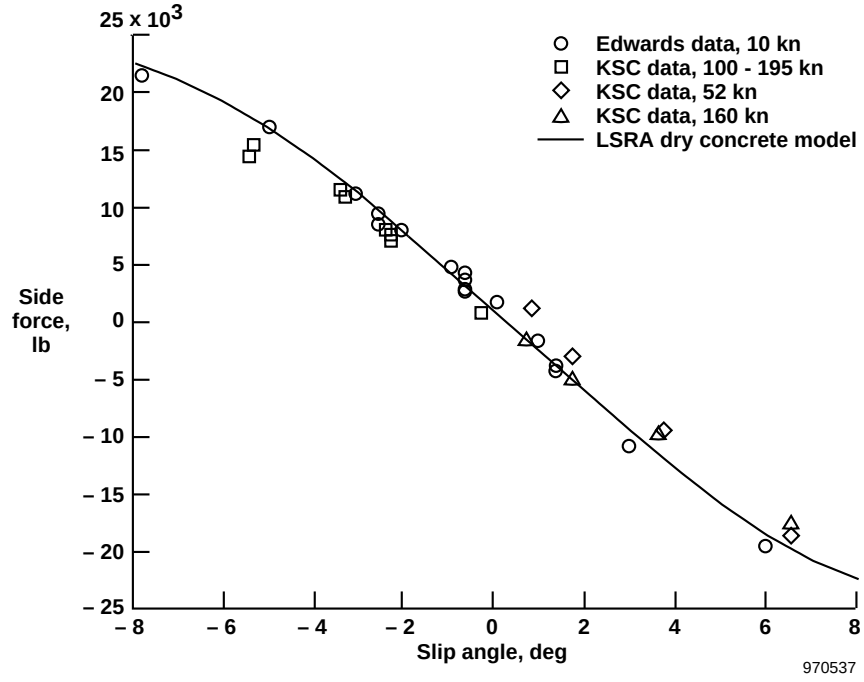

Figure 20. Main gear EAFB and KSC tire dry concrete side forces at 63,000 lb ± 2,000 lb. (These EAFB data were collected on concrete, and KSC data were collected on center section on unground concrete.)

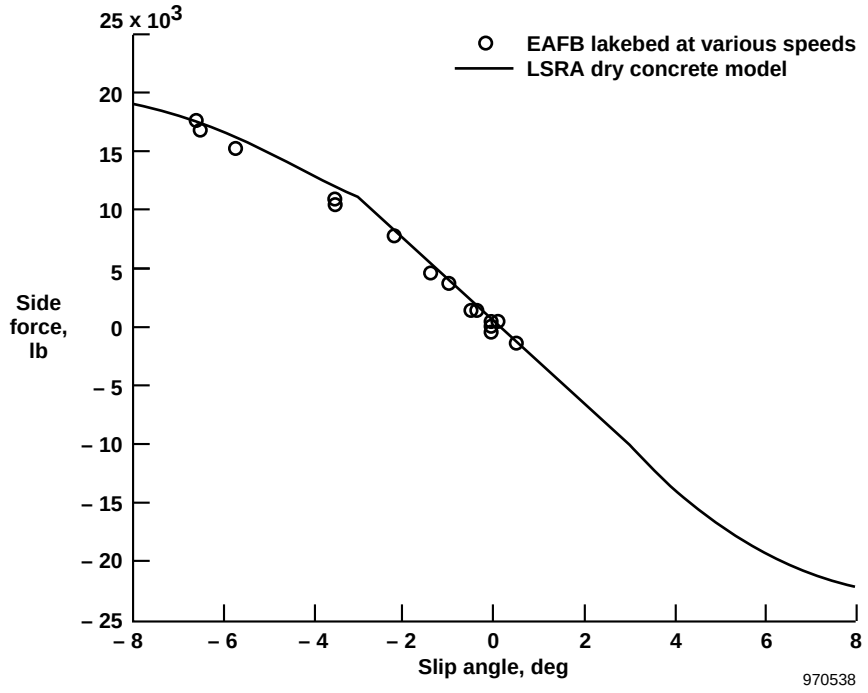

Figure 21. Main gear tire EAFB lakebed side forces at 47,000 lb.

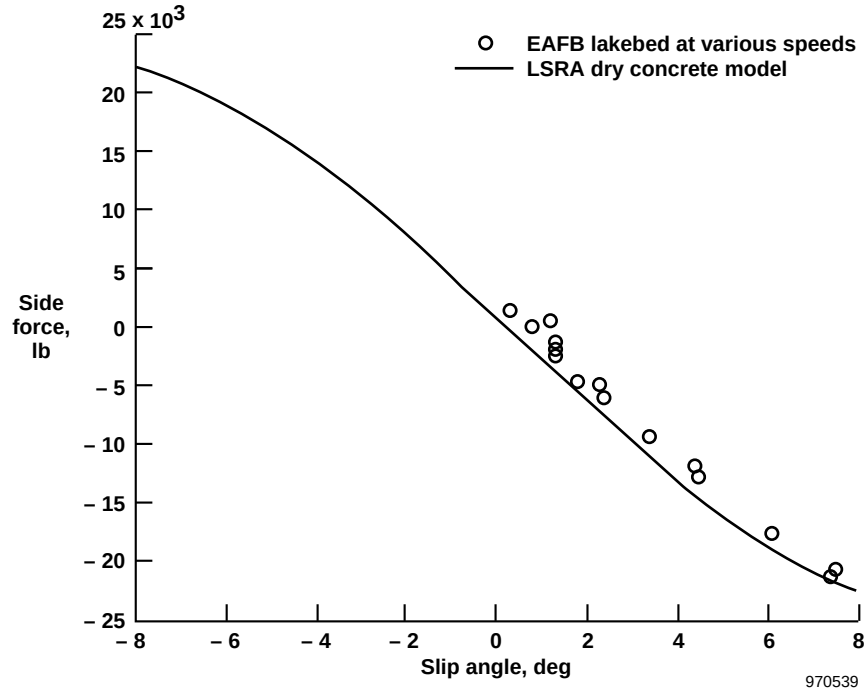

Figure 22. Main gear tire EAFB lakebed side forces at 61,000 lb.

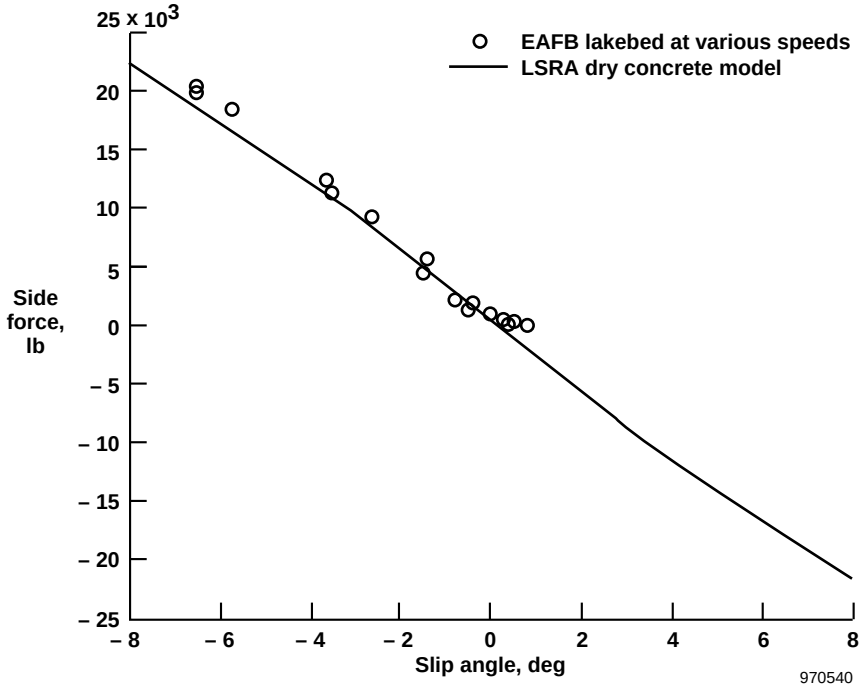

Figure 23. Main gear tire EAFB lakebed side forces at 92,000 lb.

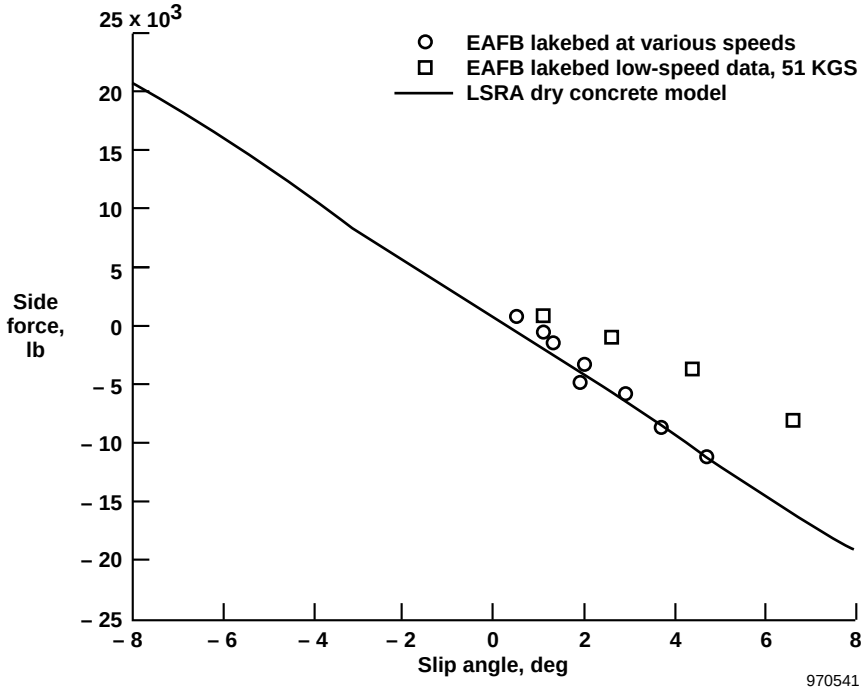

Figure 24. Main gear tire EAFB lakebed side forces at 124,000 lb.

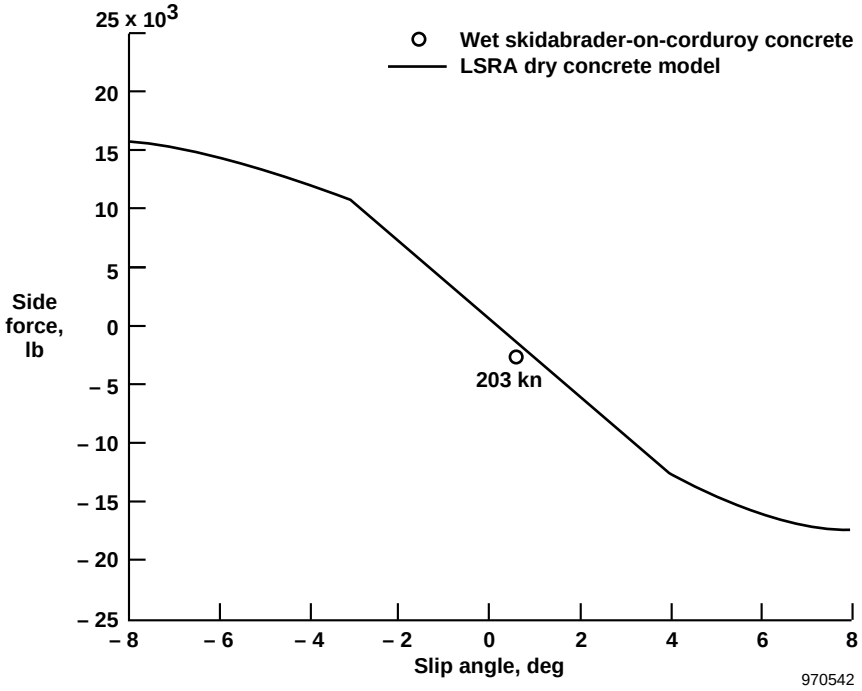

Figure 25. Main gear KSC wet concrete side forces at 36,000 lb.

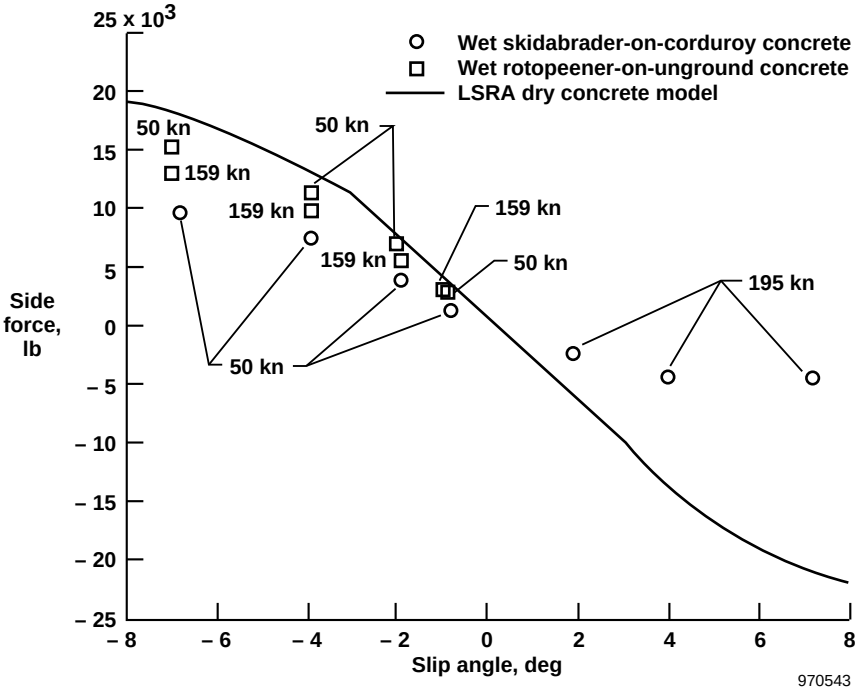

Figure 26. Main gear KSC wet concrete side forces at 47,000 lb.

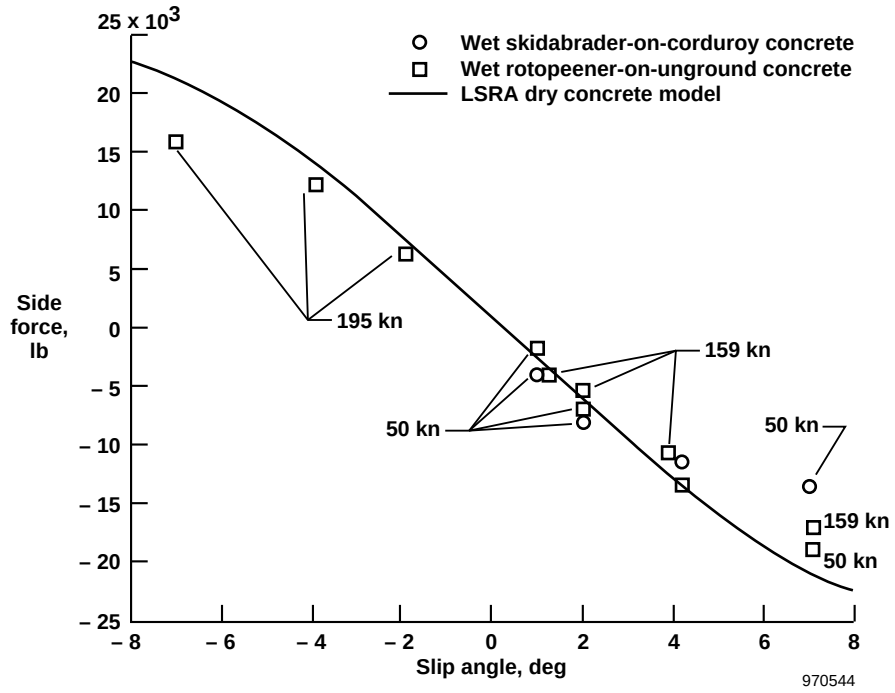

Figure 27. Main gear KSC wet concrete side forces at 63,000 lb.

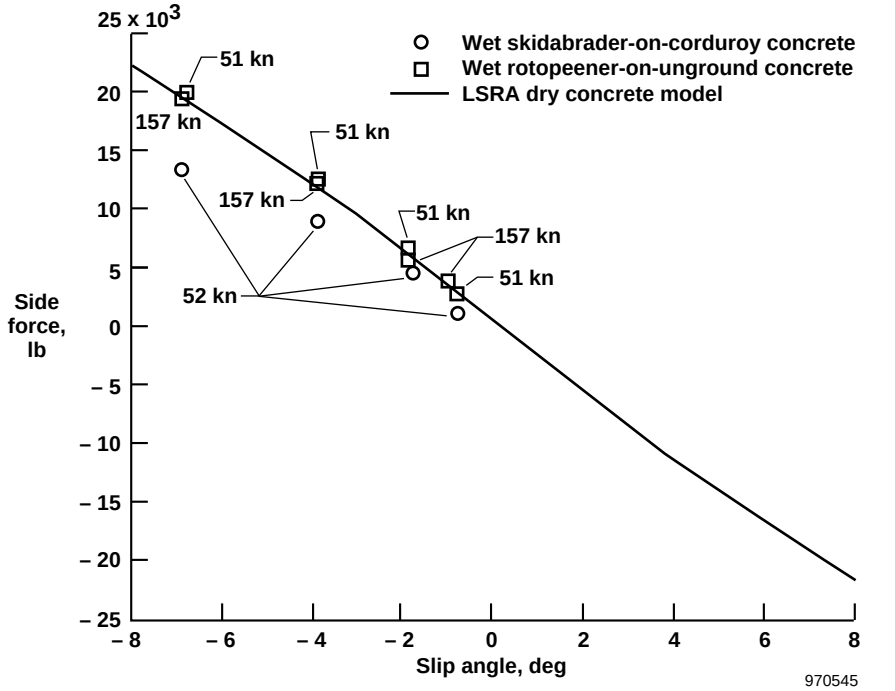

Figure 28. Main gear KSC wet concrete side forces at 93,000 lb.

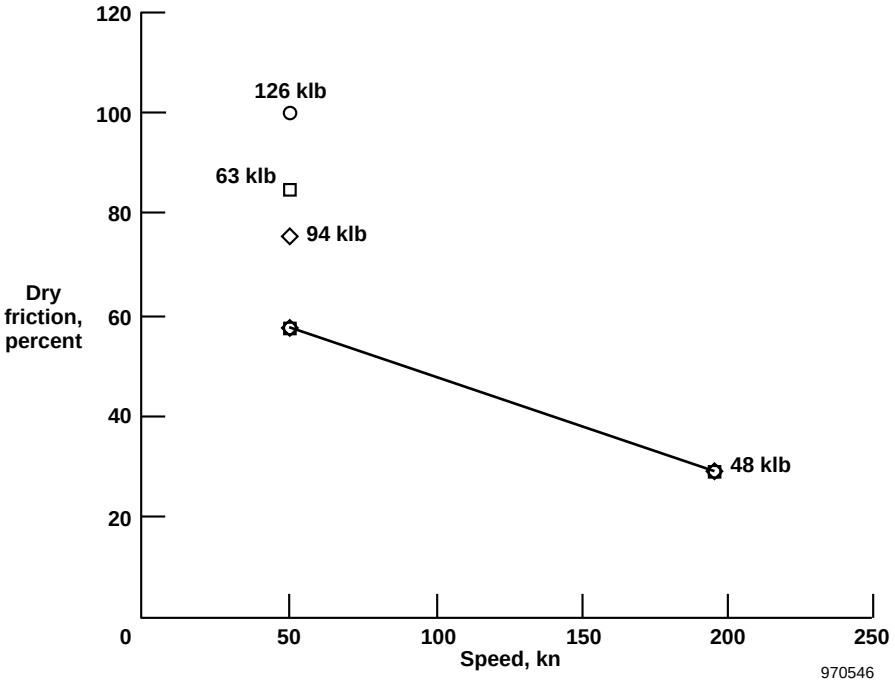

Figure 29. Main gear KSC tire side force on wet skid abraded on corduroy section as a function of dry concrete forces.

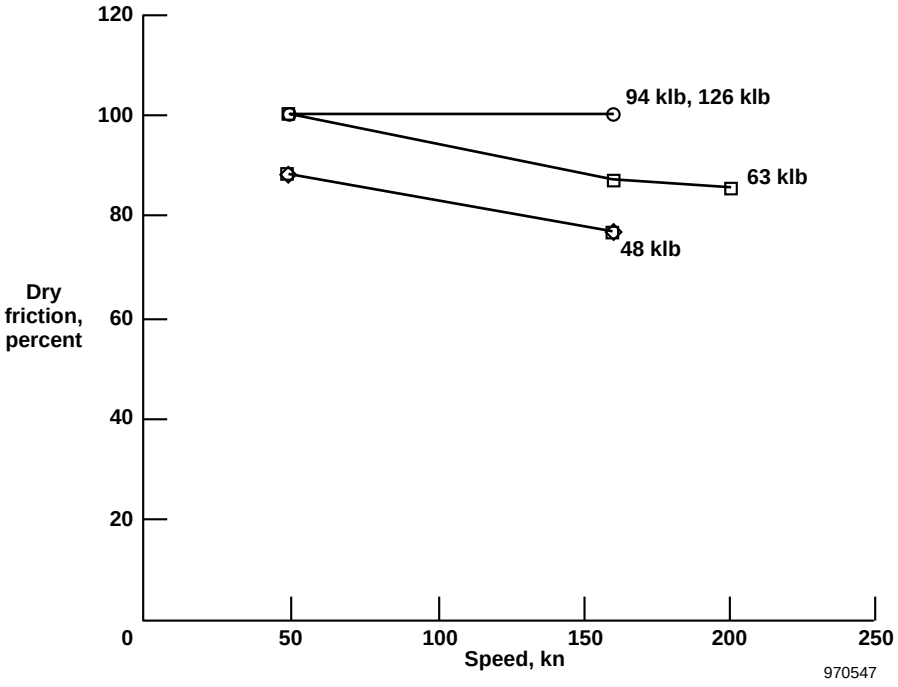

Figure 30. Main gear KSC tire side force on wet rotopeened unground section as a function of dry concrete forces.

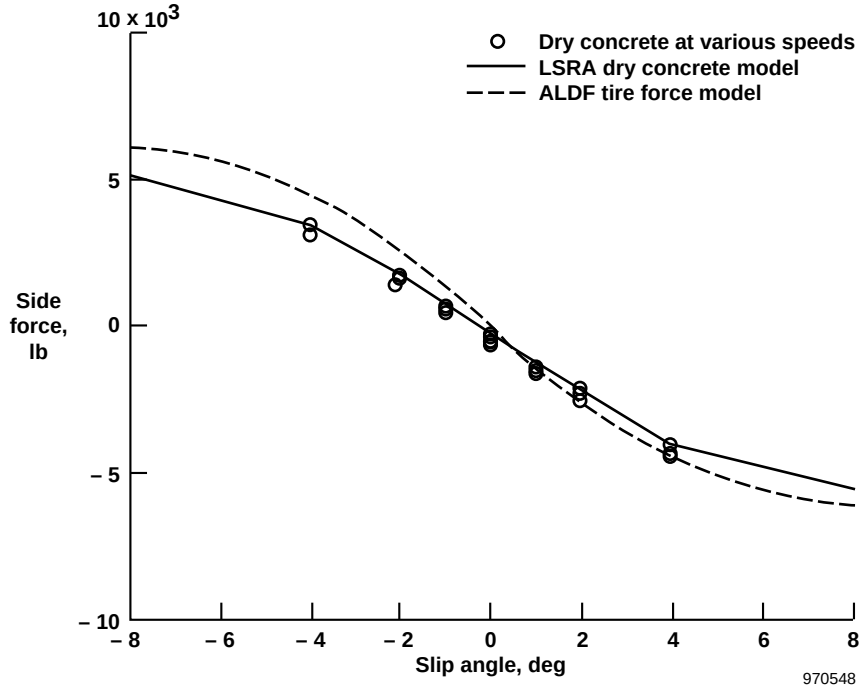

Figure 31. Nose gear EAFB dry concrete side forces at 11,000 lb.

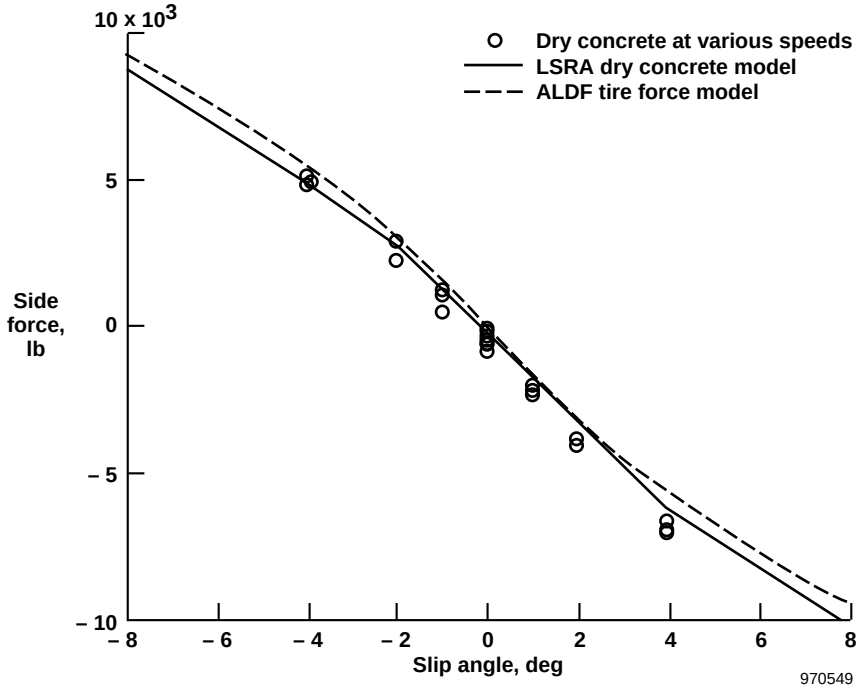

Figure 32. Nose gear EAFB dry concrete side forces at 33,000 lb.

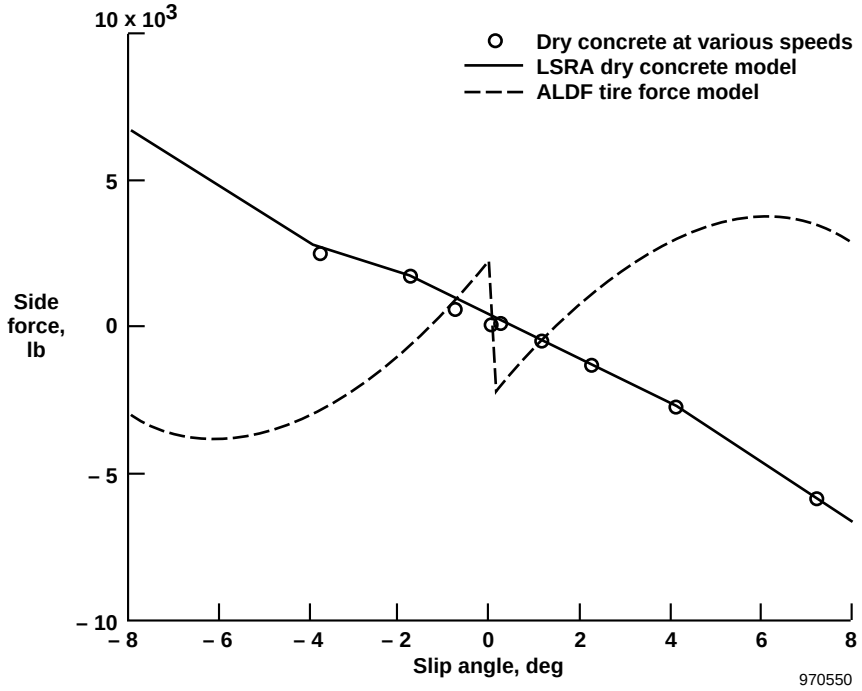

Figure 33. Nose gear EAFB dry concrete side forces at 50,000 lb.

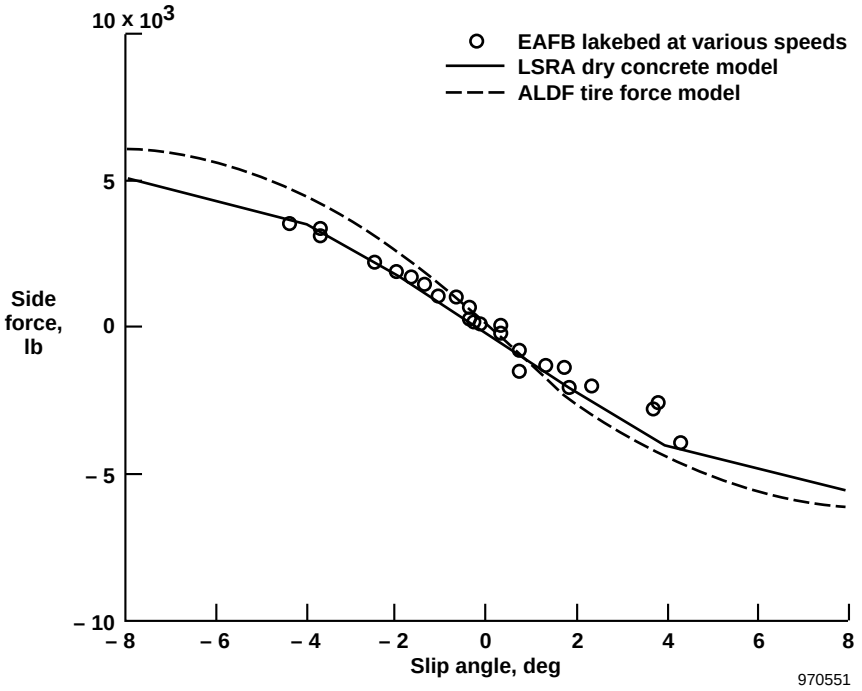

Figure 34. Nose gear EAFB lakebed side forces at 11,000 lb.

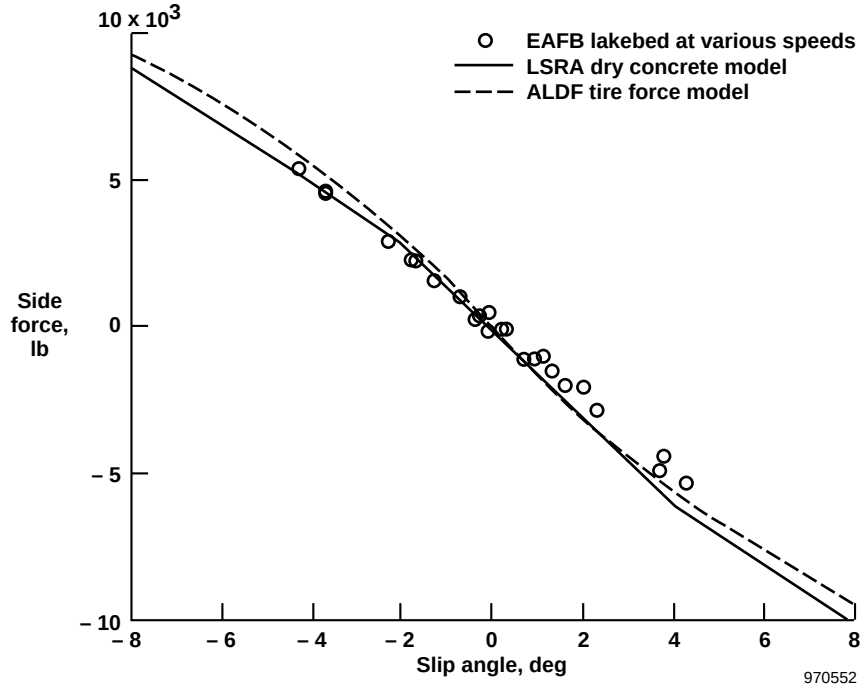

Figure 35. Nose gear EAFB lakebed side forces at 33,000 lb.

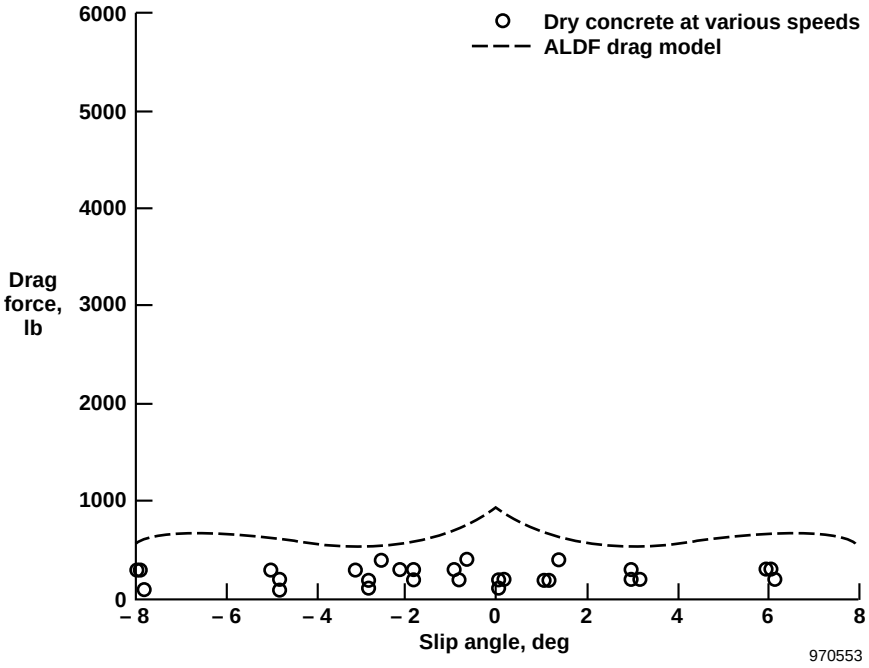

Figure 36. Main gear EAFB and KSC tire drag forces at 33,000 lb.

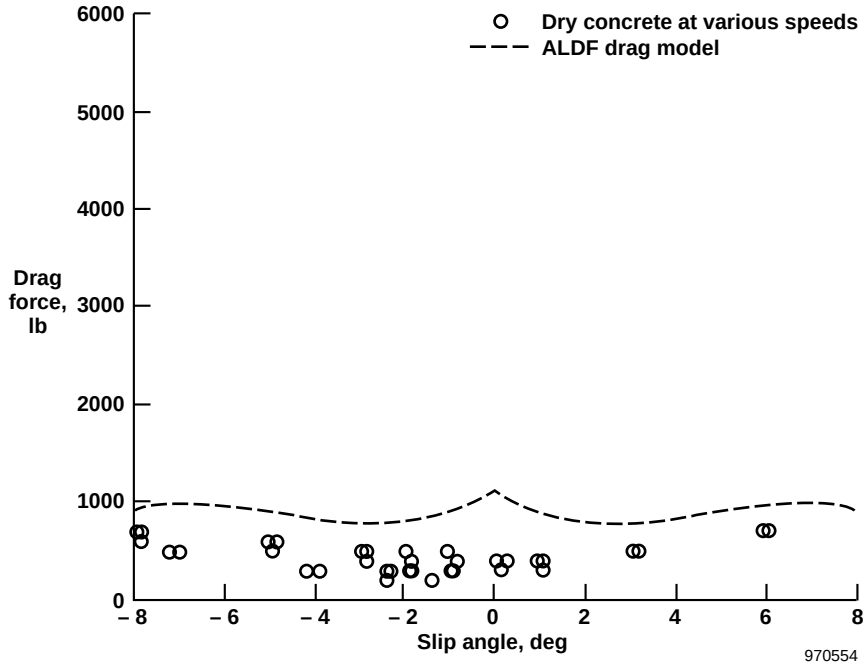

Figure 37. Main gear EAFB and KSC tire drag forces at 48,000 lb.

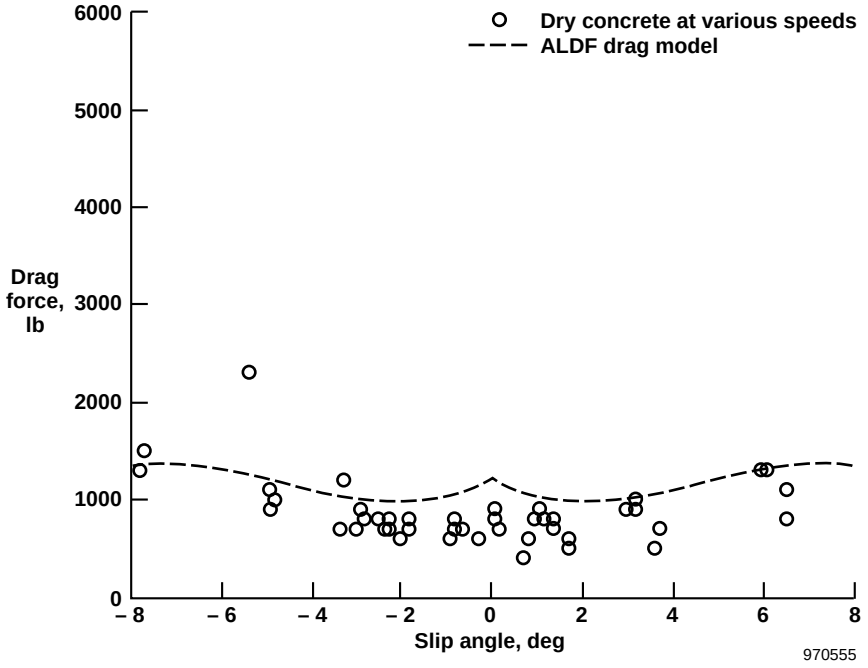

Figure 38. Main gear EAFB and KSC tire drag forces at 63,000 lb.

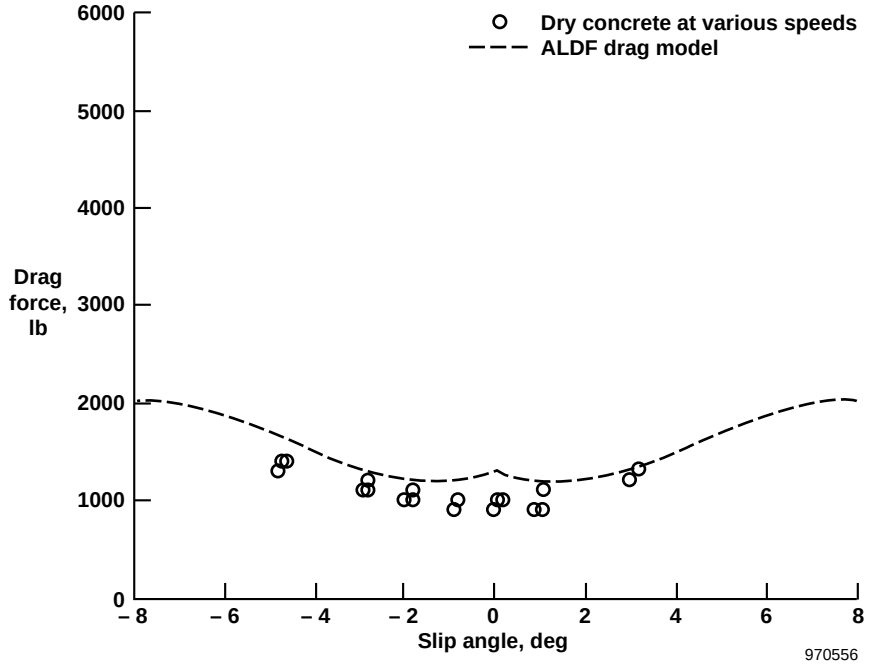

Figure 39. Main gear EAFB and KSC tire drag forces at 80,000 lb.

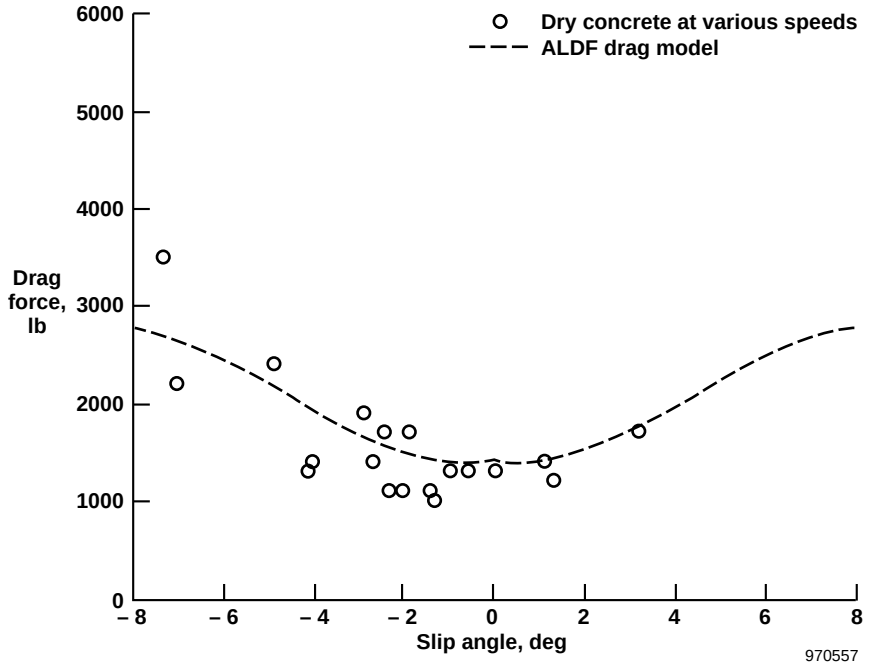

Figure 40. Main gear EAFB and KSC tire drag forces at 93,000 lb.

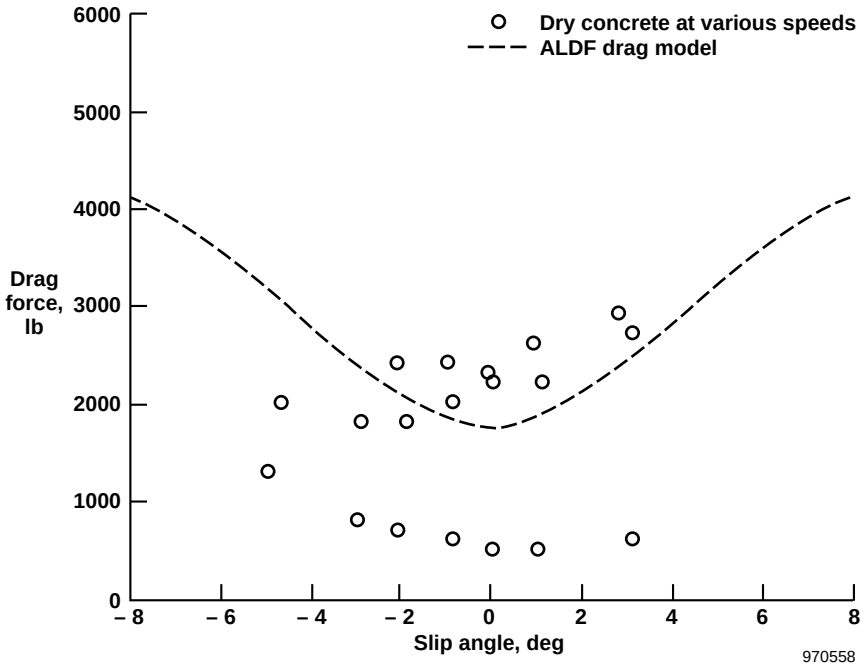

Figure 41. Main gear EAFB and KSC tire drag forces at 110,000 lb.

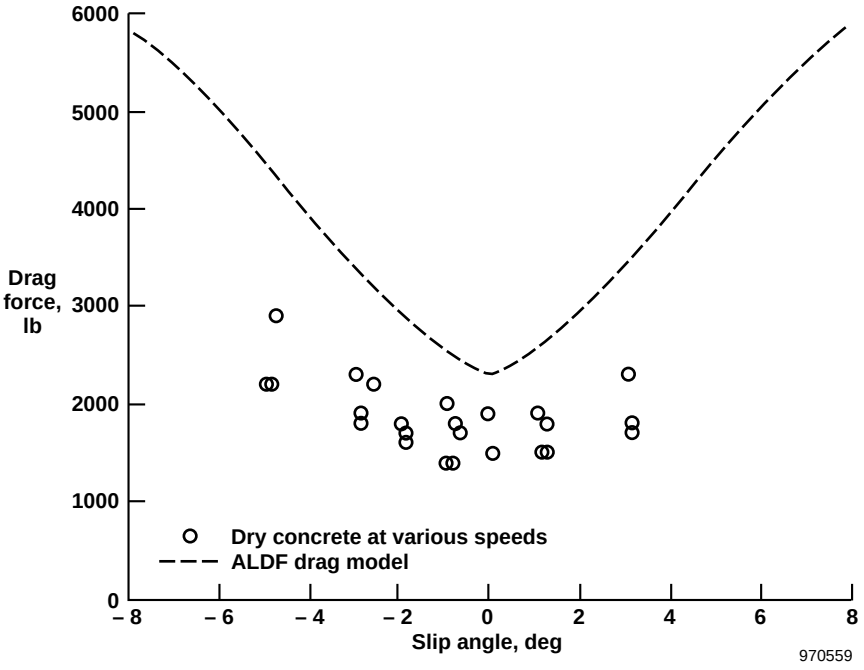

Figure 42. Main gear EAFB and KSC tire drag forces at 126,000 lb.

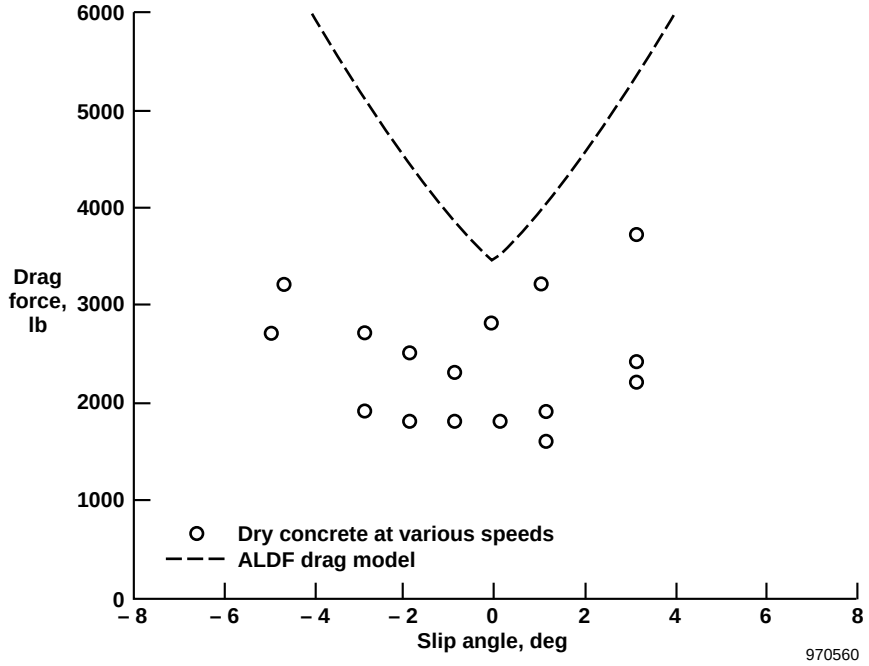

Figure 43. Main gear EAFB and KSC tire drag forces at 145,000 lb ± 4,000 lb.

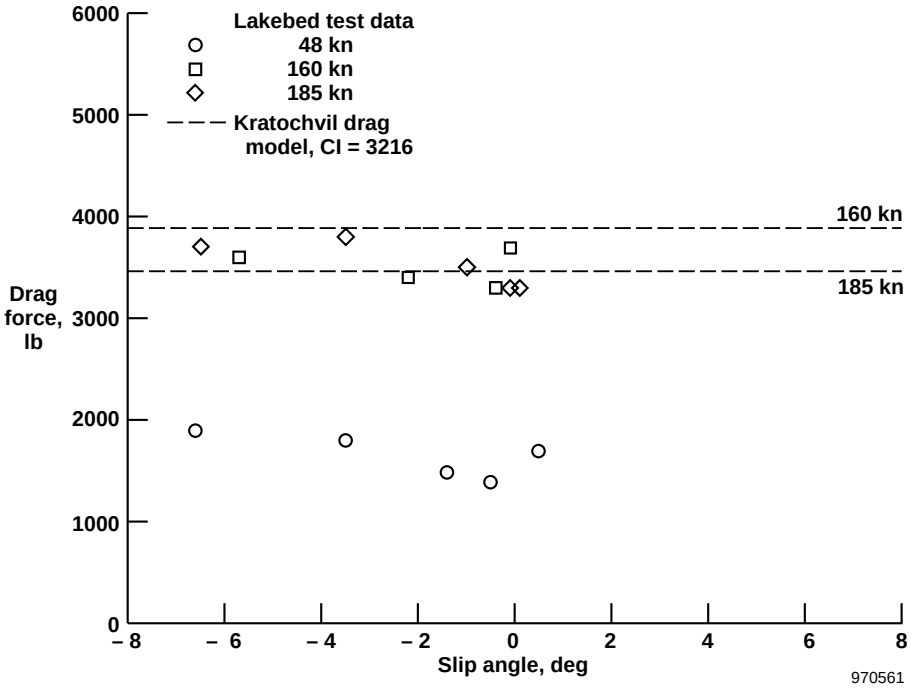

Figure 44. Main gear EAFB and KSC tire drag forces on EAFB lakebed runway 15 at 46,000 lb.

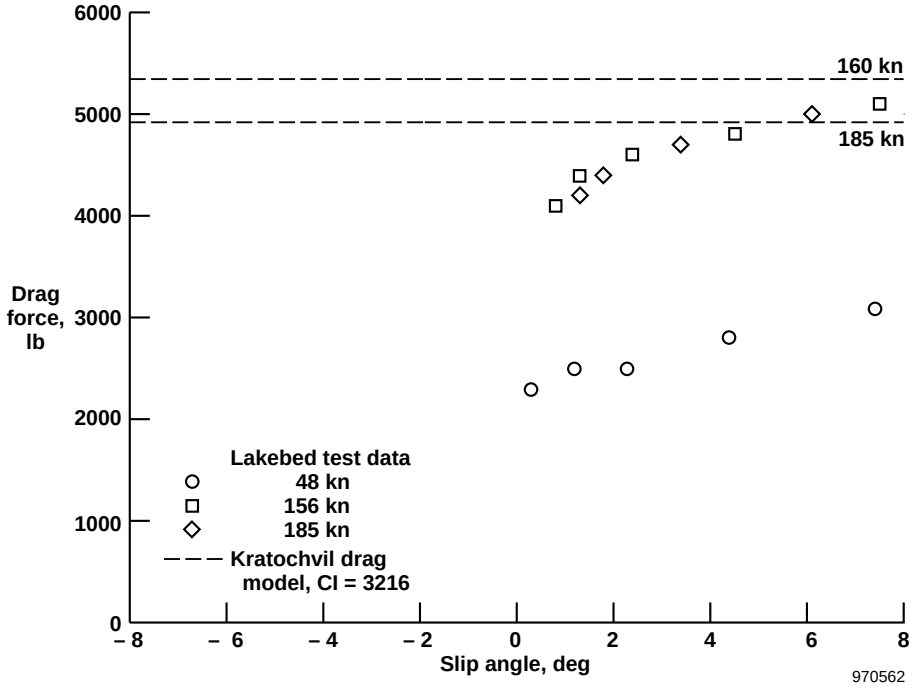

Figure 45. Main gear EAFB and KSC tire drag forces on EAFB lakebed runway 15 at 62,000 lb.

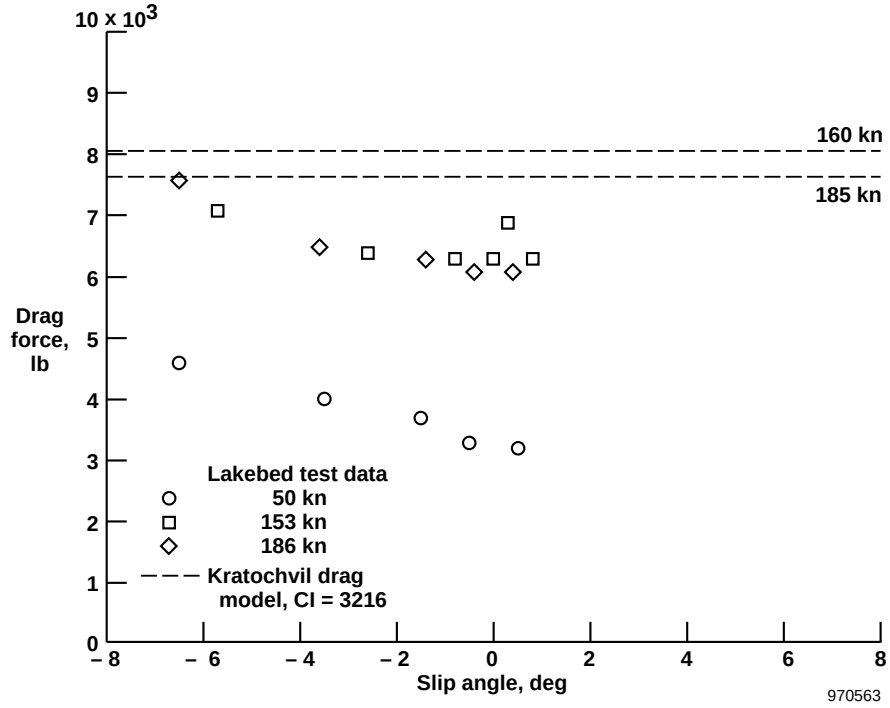

Figure 46. Main gear EAFB and KSC tire drag forces on EAFB lakebed runway 15 at 92,000 lb.

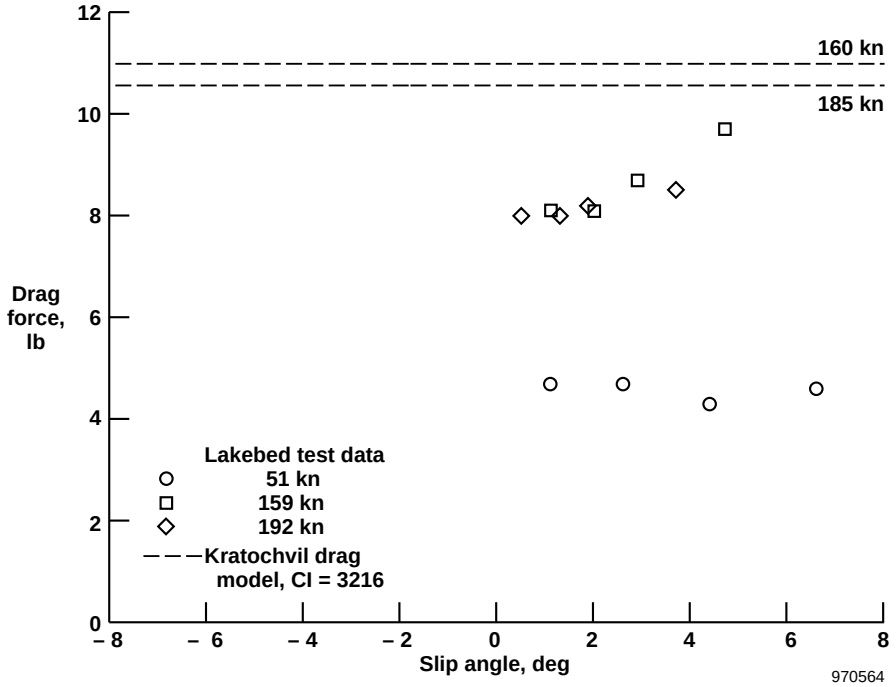

Figure 47. Main gear EAFB and KSC tire drag forces on EAFB lakebed runway 15 at 126,000 lb.

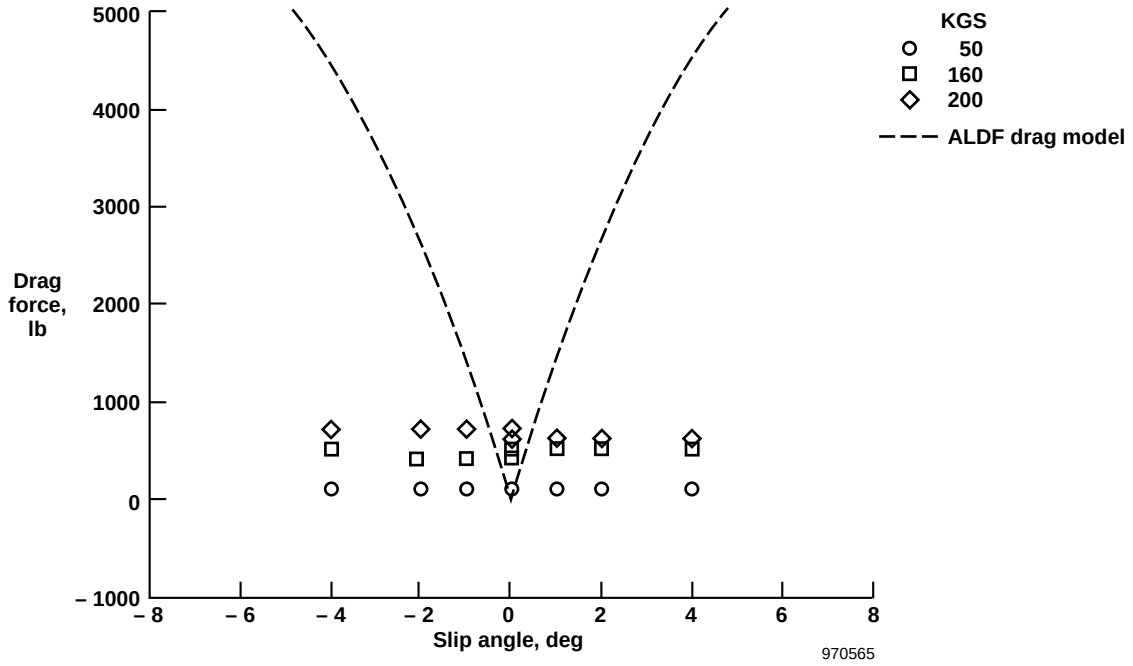

Figure 48. Nose wheel gear EAFB tire drag forces on concrete at 11,000 lb.

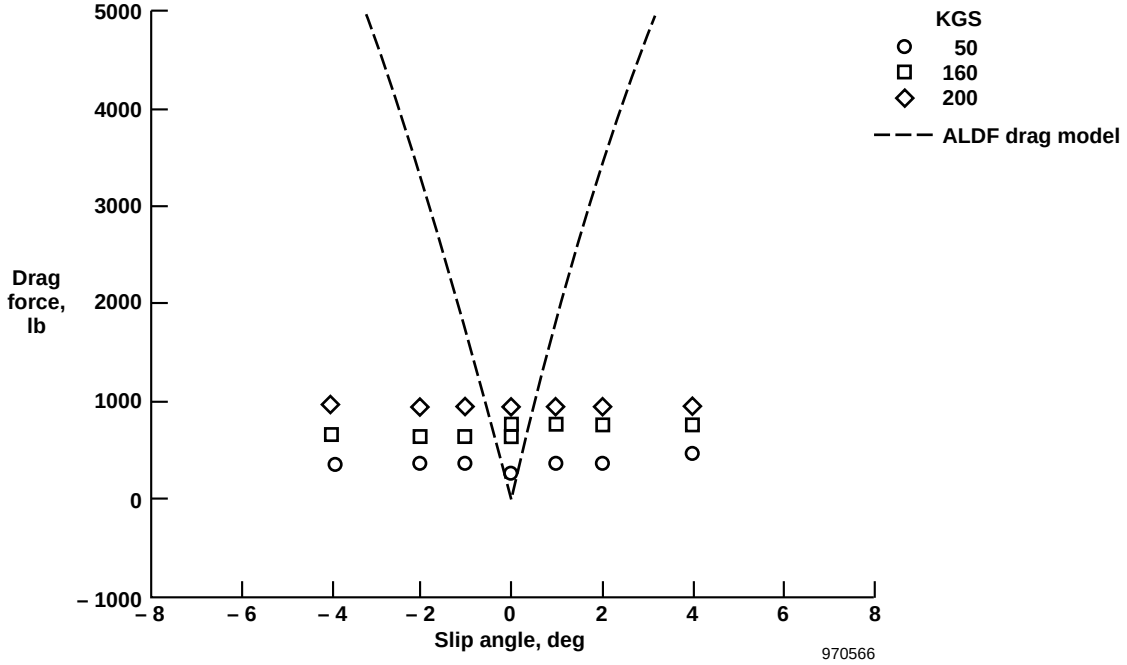

Figure 49. Nose gear EAFB tire drag forces on concrete at 31,000 lb.

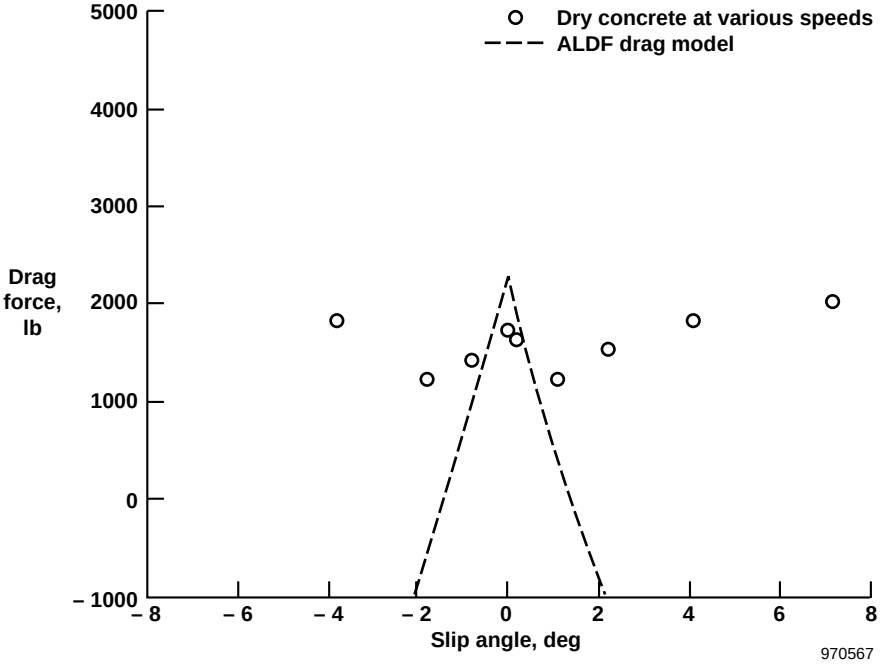

Figure 50. Nose gear EAFB tire drag forces on concrete at 50,000 lb.

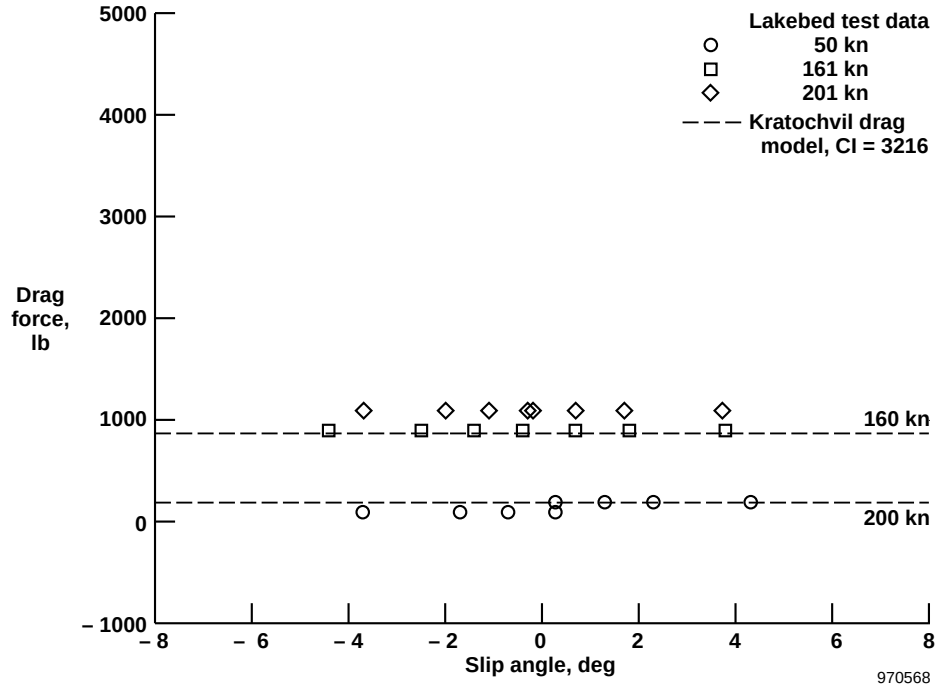

Figure 51. Nose gear EAFB tire drag forces on lakebed at 11,000 lb.

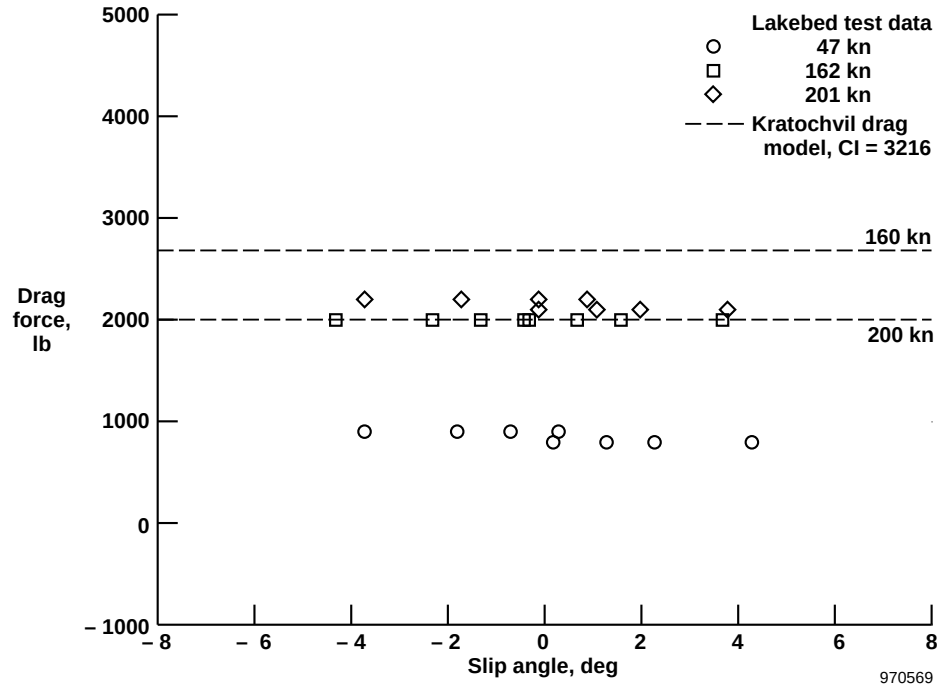

Figure 52. Nose gear EAFB tire drag forces on lakebed at 31,000 lb.

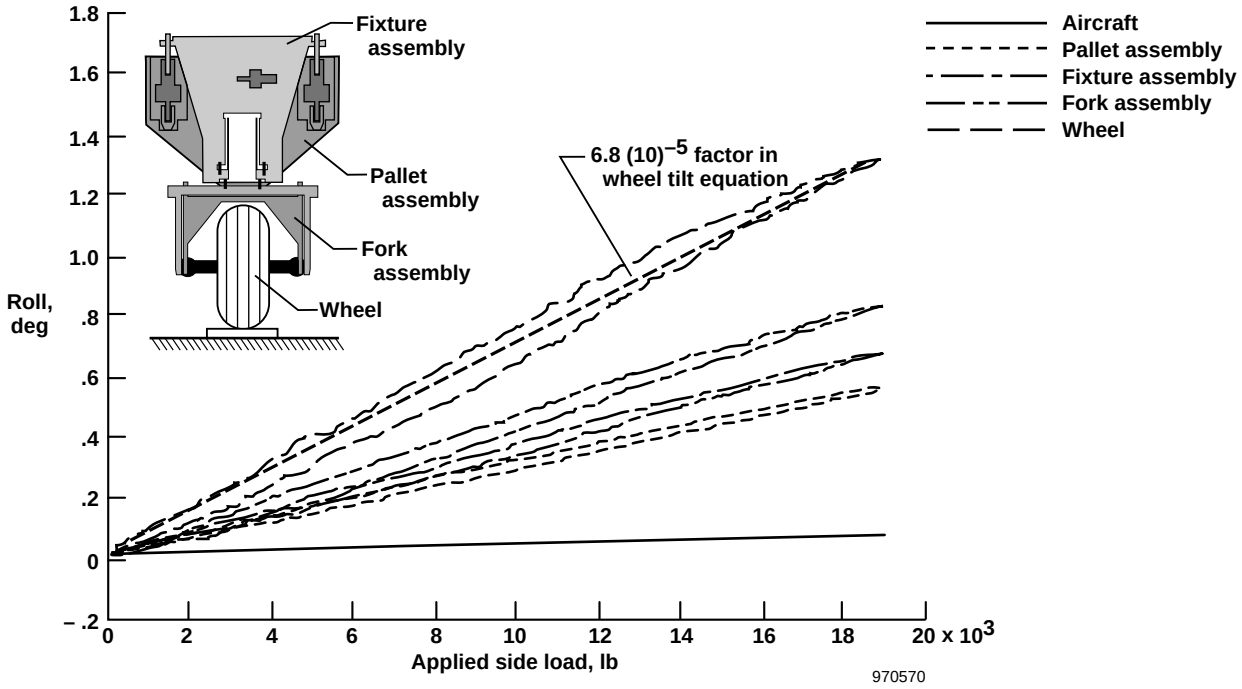

Figure B1. Measured roll deflection relative to the ground caused by side load from load point.

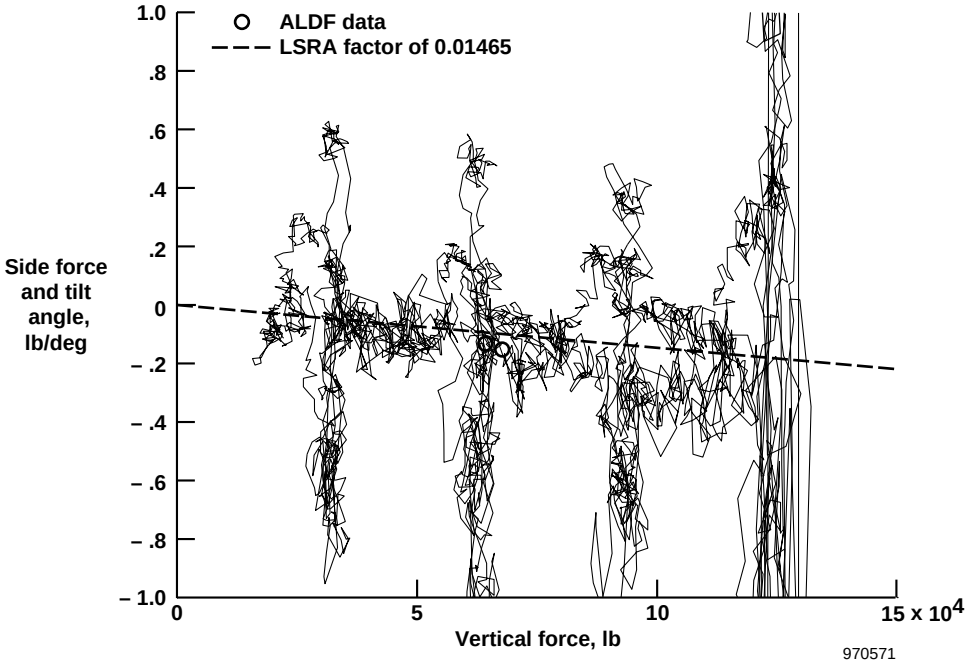

Figure B2. Measured concrete forces from LSRA tests. (Dotted line represents LSRA factor of 0.01465.)

REPORT DOCUMENTATION PAGE

Form Approved
OMB No. 0704-0188

1. AGENCY USE ONLY (Leave blank)	2. REPORT DATE	3. REPORT TYPE AND DATES COVERED
	September 1997	Technical Memorandum

4. TITLE AND SUBTITLE

A Model for Space Shuttle Orbiter Tire Side Forces Based on NASA Landing Systems Research Aircraft Test Results

5. FUNDING NUMBERS

WU 551-15-01

6. AUTHOR(S)

John F. Carter, Christopher J. Nagy, and Joseph S. Barnicki

7. PERFORMING ORGANIZATION NAME(S) AND ADDRESS(ES)

NASA Dryden Flight Research Center
P.O. Box 273
Edwards, California 93523-0273

8. PERFORMING ORGANIZATION REPORT NUMBER

H-2168

9. SPONSORING/MONITORING AGENCY NAME(S) AND ADDRESS(ES)

National Aeronautics and Space Administration
Washington, DC 20546-0001

10. SPONSORING/MONITORING AGENCY REPORT NUMBER

NASA TM-4808

11. SUPPLEMENTARY NOTES

12a. DISTRIBUTION/AVAILABILITY STATEMENT

Unclassified—Unlimited
Subject Category 05

12b. DISTRIBUTION CODE

13. ABSTRACT (Maximum 200 words)

Forces generated by the Space Shuttle orbiter tire under varying vertical load, slip angle, speed, and surface conditions were measured using the Landing System Research Aircraft (LSRA). Resulting data were used to calculate a mathematical model for predicting tire forces in orbiter simulations. Tire side and drag forces experienced by an orbiter tire are cataloged as a function of vertical load and slip angle. The mathematical model is compared to existing tire force models for the Space Shuttle orbiter. This report describes the LSRA and a typical test sequence. Testing methods, data reduction, and error analysis are presented. The LSRA testing was conducted on concrete and lakebed runways at the Edwards Air Force Flight Test Center and on concrete runways at the Kennedy Space Center (KSC). Wet runway tire force tests were performed on test strips made at the KSC using different surfacing techniques. Data were corrected for ply steer forces and conicity.

14. SUBJECT TERMS

Aircraft tire, CV-990, Landing gear, Landing system, Space shuttle orbiter test facility

15. NUMBER OF PAGES

66

16. PRICE CODE

AO4

17. SECURITY CLASSIFICATION OF REPORT	18. SECURITY CLASSIFICATION OF THIS PAGE	19. SECURITY CLASSIFICATION OF ABSTRACT	20. LIMITATION OF ABSTRACT
Unclassified	Unclassified	Unclassified	Unlimited

NSN 7540-01-280-5500

Available from the NASA Center for AeroSpace Information, 800 Elkridge Landing Road, Linthicum Heights, MD 21090; (301)621-0390

Standard Form 298 (Rev. 2-89)
Prescribed by ANSI Std. Z39-18
298-102